Electronic Stopping of Protons for Lithium in the Dielectric Formulation Obtained from First-Principles Calculations

Richard J. Mathar,[1] John R. Sabin,[2] S. B. Trickey[3]

Department of Physics, Quantum Theory Project, Univ. of Florida, Gainesville, FL 32611-8435, USA

Received 8 December 1998; revised 23 March 1999

Abstract

We calculate the wave-vector and frequency-dependent dielectric matrix of bulk crystals by use of first-principles, all-electron Kohn–Sham states in the integral of the irreducible polarizability in the random phase approximation. From this we determine the macroscopic "head" element, the $(\mathbf{0},\mathbf{0})$-element, of the inverse matrix (the energy loss function), and integrate over energy and momentum transfers to obtain the electronic energy loss of protons at low velocities. Numerical results are given for hexagonal close packed lithium.

Key words: Electronic energy loss; Protons; Dielectric Matrix; RPA.
PACS: 61.80.Jh; 34.50.Bw; 71.45.Gm

1 Dielectric Response — Bulk Crystals

1.1 Electronic Stopping

The objective of the research reported here is provision of a quantitative, materials-specific, first-principles description of the energy deposition by a single ion in an ordered material target. We consider only protons, thus avoid having to deal with the additional complication of bound electronic states of

[1] Fax +49 6221 528 246; e-mail mathar@mpia-hd.mpg.de
[2] Fax +1 352 392 8722; e-mail sabin@qtp.ufl.edu
[3] Corresponding author. Fax +1 352 392 8722; e-mail trickey@qtp.ufl.edu

Article published in Nuclear Instruments and Methods B 155 (2009) 249–293

the projectile with the associated problems of Fermi-statistics of all electrons in the projectile-target system and dynamic charge states. (Note: quite a few multi-letter abbreviations occur. An explanation of each is provided at the point of first use in the text and a list is given in Appendix E.)

For a massive classical ion with charge distribution $\rho_{\rm ext}(\mathbf{r},t)$ the energy loss per unit path length to a target in the microscopic dielectric formulation is

$$\frac{\mathrm{d}E}{\mathrm{d}x} = \frac{1}{4\pi^3\epsilon_0 v}\int \mathrm{d}^3q\,\mathbf{v}\cdot\mathbf{q}\int_0^\infty \mathrm{d}\omega\delta\left(\omega-\mathbf{q}\cdot\mathbf{v}\right) \times \sum_{\mathbf{G}\perp\mathbf{v}}\frac{1}{(\mathbf{q}+\mathbf{G})^2}\,\mathrm{Im}\left[K_{\mathbf{0},\mathbf{G}}(\mathbf{q},\omega)\rho^*_{\rm ext}(\mathbf{q})\rho_{\rm ext}(\mathbf{q}+\mathbf{G})\right]. \tag{1}$$

Appendix A derives this result (and summarizes restrictions). The more familiar form is for the limit of a punctiform ion

$$\frac{\mathrm{d}E}{\mathrm{d}x}(\mathbf{v}) = \frac{(Z_1e)^2}{4\pi^3\epsilon_0 v}\int \mathrm{d}^3q\frac{\mathbf{v}\cdot\mathbf{q}}{q^2}\int_0^\infty \mathrm{d}\omega\delta(\omega-\mathbf{q}\cdot\mathbf{v})\,\mathrm{Im}\,K_{\mathbf{0},\mathbf{0}}(\mathbf{q},\omega), \tag{2}$$

with Z_1 the projectile charge number, $\mathbf{v}$ the projectile velocity in the target rest frame, m the free electron rest mass, e the elementary charge unit, $\mathbf{G}$ denotes reciprocal lattice vectors, and ϵ_0 is the vacuum permittivity. (SI units are used in all equations.) While the detailed results presented here are restricted to the punctiform ion case, it should be clear throughout that inclusion of the spatial distribution of projectile charge is no particular obstacle.

$K_{\mathbf{0},\mathbf{0}}$ is the $\mathbf{G}=\mathbf{G}'=\mathbf{0}$ ("head") component of the inverse dielectric matrix defined by

$$\sum_{\mathbf{G}'}\epsilon_{\mathbf{G},\mathbf{G}'}(\mathbf{q},\omega)K_{\mathbf{G}',\mathbf{G}''}(\mathbf{q},\omega) = \delta_{\mathbf{G}\mathbf{G}''} \tag{3}$$

with respect to $\epsilon_{\mathbf{G}',\mathbf{G}''}(\mathbf{k},\omega)$, the frequency and wave-vector dependent microscopic dielectric matrix. An infinite number of orders in the diagrammatic expansion of the effective, screened interaction is summed if the dielectric matrix itself is derived from the irreducible polarizability Π,

$$\epsilon_{\mathbf{G},\mathbf{G}'}(\mathbf{q},\omega) = \delta_{\mathbf{G}\mathbf{G}'} - \frac{e^2}{\epsilon_0|\mathbf{q}+\mathbf{G}|^2}\Pi(\mathbf{q}+\mathbf{G},\mathbf{q}+\mathbf{G}',\omega), \tag{4}$$

given in detail below.

Early calculations of $\epsilon_{\mathbf{G},\mathbf{G}'}(\mathbf{q},\omega)$ frequently reduced the problem to a joint density of states via the approximation of constant matrix elements for the

irreducible polarizability [1], and tended to focus on the long-wavelength optical properties or the static screening, hence omitted either the frequency or wave-vector dependence [2–5]. More recent work, fueled by the Density Functional Theory (DFT) "band-gap problem" in semiconductors and insulators, has used model dielectric functions to provide the screened Coulomb potential in the *GW* approximation [6–9].

There is a vast literature of dielectric treatments of energy deposition [10–18]. The majority of papers has used variants on the theme of $\epsilon(q,\omega)$ from the homogeneous electron gas. A popular subtheme is the local plasma density approximation (LPDA) to the response of the inhomogeneous electron density in more specific target materials [19–28].

We consider the pertinent aspects of the electron population, then calculate the desired energy deposition cross section from that microscopic knowledge. The potential impact of system structure upon electronic response is illustrated by crystalline aluminum. Experimentally a decrease of only 8% in lattice constant (achieved at 310 kbar) causes a drastic qualitative change in the optical conductivity [29]: one peak at about 1.5 eV splits into two (at 1.5 and 2.5 eV).

1.2 Density Functional Theory Implementation

We determine the ground-state electronic structure of solids within DFT as established in the Kohn–Sham (KS) variational procedure. The KS equations in the local density approximation to the potential $V[\rho(\mathbf{r})]$ are

$$\left\{-\frac{\hbar^2}{2m}\nabla^2 + V[\rho(\mathbf{r})]\right\}\varphi_{\nu,\mathbf{k}}(\mathbf{r}) = E_{\nu,\mathbf{k}}\varphi_{\nu,\mathbf{k}}(\mathbf{r}). \tag{5}$$

(The symbol $E_{\nu,\mathbf{k}}$ is used for the KS eigenvalues rather than the common $\varepsilon_{\nu,\mathbf{k}}$ of the DFT literature to set them apart from matrix components $\epsilon_{\mathbf{G},\mathbf{G}'}$.) The electron number density ρ is given by

$$\rho(\mathbf{r}) = V_{\mathrm{UC}}\sum_{\nu}\int_{\mathrm{UC}}\frac{\mathrm{d}^3k}{(2\pi)^3}f_{\nu,\mathbf{k}}|\varphi_{\nu,\mathbf{k}}(\mathbf{r})|^2 \tag{6}$$

in terms of the eigenfunctions $\varphi_{\nu,\mathbf{k}}$ and occupation numbers $f_{\nu,\mathbf{k}}$, which depend on band indices ν and wave vectors $\mathbf{k}$. V_{UC} denotes the volume of a unit cell (UC). Spin dependencies have been removed from the notation, since the present application uses only the spin-degenerate (non–spin-polarized) case with $f_{\nu,\mathbf{k}} = 0$ or 2 for $E_{\nu,\mathbf{k}}$ above or below the Fermi energy E_{F}. The potentials

$V[\rho(\mathbf{r})]$ contain electron-electron Coulomb repulsion, exchange-correlation, and nuclear-electron attraction terms. The results that follow use the Moruzzi–Janak–Williams parameterization [30] of the Hedin–Lundqvist local-density approximation (LDA) to the exchange-correlation potential.

We use the computational package GTOFF [31–36] to solve the KS equations. It performs all-electron, full-potential, linear combination of Gaussian Type Orbitals (GTO's) calculations via Fitting Function algorithms [37–39]. Those algorithms handle the non-linear dependence of the KS potentials upon the spin densities (hence, upon the KS orbitals) via intermediate linear expansion in an auxiliary Gaussian basis set and accelerate the Coulomb integrals by an auxiliary expansion as well. There are no pseudopotentials or frozen cores (which would prevent the inclusion of core-shell excitations in the stopping-power analysis or demand special handling [40]), nor muffin-tin potentials.

The task is to solve the KS equations and determine the electronic structure of lowest energy for given lattice parameters, then use the KS orbitals and eigenvalue differences to construct Π. Such use of the KS orbitals and eigenvalues is not rigorous, but has proven to be quite reasonable in both *GW* calculations and in other studies which tested the issue [41–43].

1.3 RPA and Matrix Elements

In the Random Phase Approximation, the retarded form of Π is [44–46] [4]

$$\begin{aligned}&\Pi(\mathbf{q}+\mathbf{G},\mathbf{q}+\mathbf{G}',\omega)\\&=\sum_{\nu\nu'}\int_{\mathrm{BZ}}\frac{\mathrm{d}^3k}{(2\pi)^3}\,\frac{m^*_{\mathbf{G}}m_{\mathbf{G}'}(f_{\nu\mathbf{k}}-f_{\nu'\mathbf{k}+\mathbf{q}})}{\hbar\omega+\mathrm{i}\eta+E_{\nu\mathbf{k}}-E_{\nu'\mathbf{k}+\mathbf{q}}}\end{aligned}\tag{7}$$

where ν,ν' are band indices and $E_{\nu,\mathbf{k}}$ the band dispersions. The integral is over the first Brillouin zone (BZ), but can be evaluated equivalently (and more conveniently) over a primitive unit cell of the reciprocal lattice, since the integrand is a periodic function of $\mathbf{k}$. The sum is over all non-ordered band pairs; the terms $\nu<\nu'$ may be rewritten as a sum over ordered pairs $\nu>\nu'$ with a simultaneous change of the sign of $\hbar\omega$ [47].

The matrix elements in Eq. (7) are given by

$$m_{\mathbf{G}}\equiv\langle\nu'\mathbf{k}+\mathbf{q}|\,\mathrm{e}^{\mathrm{i}(\mathbf{G}+\mathbf{q})\cdot\mathbf{r}}\,|\nu\mathbf{k}\rangle.$$

[4] In Ref. [44], Eqs. (2.11)–(2.12) are inconsistent with Eqs. (2.7)–(2.10). Either fields ϕ must be replaced by charge densities ρ in (2.11)–(2.12), or all factors of squared wavenumbers be dropped.

Identification of the lattice-periodic part u of the Bloch functions

$$\langle \mathbf{r}|\nu\mathbf{k}\rangle = \psi_{\nu,\mathbf{k}}(\mathbf{r}) = \mathrm{e}^{\mathrm{i}\mathbf{k}\mathbf{r}}\, u_{\nu\mathbf{k}}(\mathbf{r})$$

and their plane wave (PW) expansion coefficients,

$$u_{\nu\mathbf{k},\mathbf{G}} \equiv \int_{\mathrm{UC}} \mathrm{e}^{-\mathrm{i}\mathbf{G}\cdot\mathbf{r}}\, u_{\nu\mathbf{k}}(\mathbf{r})\, \mathrm{d}^3 r, \tag{8}$$

gives a sum of the correlation type [48],

$$\begin{aligned} m_{\mathbf{G}} &= \frac{1}{V_{\mathrm{UC}}} \sum_{\mathbf{K}} u^*_{\nu',\mathbf{k}+\mathbf{q},\mathbf{K}}\, u_{\nu,\mathbf{k},\mathbf{K}-\mathbf{G}} \\ &= \frac{1}{V_{\mathrm{UC}}} \sum_{\mathbf{K}} u^*_{\nu',\mathbf{k}+\mathbf{q}+\mathbf{G},\mathbf{K}}\, u_{\nu,\mathbf{k},\mathbf{K}}. \end{aligned}$$

The simple interpretation in the extended zone scheme is that all momentum components $\hbar(\mathbf{k}+\mathbf{K})$ of a Bloch state $|\nu\mathbf{k}\rangle$ simultaneously exchange momentum $\hbar(\mathbf{q}+\mathbf{G})$ with the field and are overlapped with $|\nu'\mathbf{k}+\mathbf{q}\rangle$. The computational strategy adopted here is to transform the states from the GTO basis to a PW basis, hence gain speed from the simplicity of the formulation at the cost of storage. Alternatives are known [49–52]; the evaluation in real space would yield a lattice-sum over terms similar to those known from Cartesian GTO's [53–55]. [5]

The scaling properties of quantities in Eqs. (2) and (7) in the limit of isolated, finite-size molecular targets (gases) are identified by increasing the lattice constants and V_{UC} to infinity, which shrinks the volume of the BZ to zero. The product $N_2 V_{\mathrm{UC}}$ (with N_2 the number density of the target atoms), i.e., the number of formula units in the UC, is kept constant, but the distance between the molecules that constitute the basis of the UC increases. With no residual overlap between the molecules left, the band-structure becomes the flat, dispersionless line spectrum of an individual molecule surrounded by the vacuum. $E_{\nu,\mathbf{k}}$, $f_{\nu,\mathbf{k}}$, and the matrix elements $m_{\mathbf{G}}$ all lose their $\mathbf{k}$-dependence. Reciprocal lattice vectors become continuous variables, as the polarization density is no longer forced to respond to the external field modulo a discrete set of allowed umklapp-processes. The integral operator $\int \mathrm{d}^3k/(2\pi)^3$ in Eq. (7) is first replaced by $\sum_{\mathbf{k}}$ divided by the volume of the crystal (periodic boundary conditions), then by the factor $1/V_{\mathrm{UC}}$, whereupon the susceptibility and $\mathrm{d}E/\,\mathrm{d}x \propto O(1/V_{\mathrm{UC}})$ both approach zero. (The free path length between ion-target collisions becomes infinite in the vacuum. The dielectric function

[5] In Ref. [53], the whole exponent must be divided by γ in Eq. (A.8), not only the number 2. A factor $N_{l_2 m_2 n_2}$ is missing at the r.h.s. of Eq. (A.13).

and the index of refraction become 1.) The atomic cross section S generally is related to the energy loss by

$$S(\mathbf{v}) \equiv -\frac{1}{N_2}\frac{\mathrm{d}E}{\mathrm{d}x}. \tag{9}$$

$S \propto 1/(N_2 V_{\mathrm{UC}})$ maintains a finite value of $O(1)$, though $(\mathrm{d}E/\mathrm{d}x)/N_2$ approaches the form 0/0. [See App. B for additional observations on the interpretation of Eq. (9).] As long as the wavelength $\mathbf{q}$ of the external field is non-zero, the results depend on two different wave vectors $\mathbf{G}$ and $\mathbf{G}'$, which describe the directional dependence of the energy loss function of molecules. Going through this procedure (the removal of the translational symmetry in the spirit of an embedding in supercells of huge lattice constant) in only one dimension leads to systems with two-dimensional crystallinity, to diperiodic groups etc., which may be useful to overcome restrictions of the specular reflection model [56–59].

The Lindhard dielectric function [60,61] is recovered in the opposite limit of zero lattice constants, infinitely large BZ, one band $\nu = \nu'$, free-electron dispersion $E_{\nu\mathbf{k}} = (\hbar k)^2/(2m)$ and a constant $u_{\nu\mathbf{k}}(\mathbf{r})$.

1.4 Symmetries

1.4.1 Space Group; Time Inversion

The symmetry of the one-particle potential in the KS equation Eq. (5) with respect to a space group operation — specified by a point group operation O, translation $\mathbf{w}$, and Seitz symbol $\{O|\mathbf{w}\}$ —

$$\{O|\mathbf{w}\}V(\mathbf{r}) \equiv V(O^{-1}(\mathbf{r}-\mathbf{w})) = V(\mathbf{r})$$

establishes a corresponding symmetry of the Bloch functions [62,63]

$$u_{\nu\mathbf{k},\mathbf{G}} = \mathrm{e}^{\mathrm{i}O\mathbf{G}\cdot\mathbf{w}} u_{\nu O\mathbf{k},O\mathbf{G}}. \tag{10}$$

In addition, the time-inversion symmetry of the KS equation [i.e., $V[\rho]$ in Eq. (5) is real] leads to the independent relation [48]

$$u_{\nu-\mathbf{k},-\mathbf{G}} = u^*_{\nu\mathbf{k},\mathbf{G}}. \tag{11}$$

Fortunately, the density in Eq. (6) and the products $m^*_{\mathbf{G}} m_{\mathbf{G}'}$ in Eq. (7) are invariant under $\mathbf{k}$-dependent phase transformations $u_{\nu\mathbf{k}}(\mathbf{r}) \rightarrow \mathrm{e}^{\mathrm{i}\tau(\mathbf{k})}\, u_{\nu\mathbf{k}}(\mathbf{r})$.

For that reason it is unnecessary to "smooth" the unpredictably fluctuating complex phases of the "raw" eigenvectors $\varphi_{\nu,\mathbf{k}}(\mathbf{r})$, each produced on its own by a numerical diagonalization routine, along paths through the BZ. It is unnecessary inside both the DFT step of the calculation (here GTOFF) and in the subsequent calculation of the RPA matrix elements, though *individually* the $m_{\mathbf{G}}$ depend on these random phase factors. A proposal for enforcing a steady phase $\tau(\mathbf{k})$ is found in [64, Chapt. (3.6.2)].

The last two equations are used in fact to link the u-values in the BZ to those of the "irreducible" wedge of the BZ (IBZ), as emphasized in Sect. 1.5.3 below. A problem of assignment of the correct sign of $\mathbf{w}$ seems to arise in some cases; see App. C.

If Eq. (10) is inserted into the RPA expression (7), the space group symmetries devolve upon the irreducible polarizability and the dielectric matrix as

$$\epsilon_{\mathbf{G},\mathbf{G}'}(\mathbf{q},\omega) = \mathrm{e}^{\mathrm{i}O(\mathbf{G}-\mathbf{G}')\cdot\mathbf{w}}\,\epsilon_{O\mathbf{G},O\mathbf{G}'}(O\mathbf{q},\omega), \tag{12}$$

$$K_{\mathbf{G},\mathbf{G}'}(\mathbf{q},\omega) = \mathrm{e}^{\mathrm{i}O(\mathbf{G}-\mathbf{G}')\cdot\mathbf{w}}\,K_{O\mathbf{G},O\mathbf{G}'}(O\mathbf{q},\omega). \tag{13}$$

Since the external and induced potentials are real functions of $\mathbf{r}$ and t, we have [65]

$$\epsilon_{\mathbf{G},\mathbf{G}'}(\mathbf{q},\omega) = \epsilon^{*}_{-\mathbf{G},-\mathbf{G}'}(-\mathbf{q},-\omega). \tag{14}$$

Finally, Eq. (11) is needed to prove the following, less obvious symmetry (note the matrix transposition)

$$\epsilon_{\mathbf{G},\mathbf{G}'}(\mathbf{q},\omega) = \epsilon^{*}_{\mathbf{G}',\mathbf{G}}(\mathbf{q},-\omega).$$

For large $|\mathbf{q}|$, the following shift property enables coverage in terms of elements at smaller vectors, to wit

$$\epsilon_{\mathbf{G},\mathbf{G}'}(\mathbf{q},\omega) = \epsilon_{\mathbf{G}+\mathbf{G}'',\mathbf{G}'+\mathbf{G}''}(\mathbf{q}-\mathbf{G}'',\omega) \qquad \forall\mathbf{G}''.$$

These symmetry properties are also valid for the product $|\mathbf{q}+\mathbf{G}|^2\epsilon_{\mathbf{G},\mathbf{G}'}(\mathbf{q},\omega)$, which exhibits less singular behavior in the long wavelength limit than the dielectric matrix itself. The inverse dielectric matrix K has corresponding features [66].

The dielectric matrix is Hermitian if the product of matrix elements in Eq. (7) is real, a property which can be attained, for example, by moving the origin of the real-space coordinate system to an inversion center of $V(\mathbf{r})$ (if such a

center exists, as for hexagonal lithium and diamond). It is also Hermitian in the static limit [67,68].

Invariances with respect to the little group of $\mathbf{q}$ have not been exploited. The accelerations which would result would be restricted to points of high symmetry, therefore of dwindling value with increasing density of reciprocal space meshes.

1.4.2 Channeling

A shift of the origin of the unit cell (UC) by a vector $\mathbf{b}$ changes the phase of the Fourier Transform (FT) of the Bloch functions, the matrix elements, and the non-diagonal elements of the irreducible polarizability and dielectric matrix [5,68]:

$$\begin{aligned} u_{\nu\mathbf{k}}(\mathbf{r}) &\Rightarrow u_{\nu\mathbf{k}}(\mathbf{r}+\mathbf{b}), \\ u_{\nu\mathbf{k},\mathbf{G}} &\Rightarrow \mathrm{e}^{\mathrm{i}\mathbf{G}\cdot\mathbf{b}}\, u_{\nu\mathbf{k},\mathbf{G}}, \\ m_{\mathbf{G}} &\Rightarrow \mathrm{e}^{-\mathrm{i}\mathbf{G}\cdot\mathbf{b}}\, m_{\mathbf{G}}, \\ \epsilon_{\mathbf{G},\mathbf{G}'}(\mathbf{q},\omega) &\Rightarrow \mathrm{e}^{\mathrm{i}(\mathbf{G}-\mathbf{G}')\cdot\mathbf{b}}\, \epsilon_{\mathbf{G},\mathbf{G}'}(\mathbf{q},\omega), \\ K_{\mathbf{G},\mathbf{G}'}(\mathbf{q},\omega) &\Rightarrow \mathrm{e}^{\mathrm{i}(\mathbf{G}-\mathbf{G}')\cdot\mathbf{b}}\, K_{\mathbf{G},\mathbf{G}'}(\mathbf{q},\omega). \end{aligned} \tag{15}$$

The function $\mathrm{Im}\, K_{\mathbf{0},\mathbf{0}}(\mathbf{q},\omega)$ remains unaffected. However channeling calculations [69–74] [6] specify microscopic, detailed "classical" ion paths and impact parameters through these interfering phase factors by accumulation of some elements $K_{\mathbf{G}\neq\mathbf{G}'}$ as formulated in Eq. (1).

1.4.3 Hermitian Form

To avoid confusion we mention that a different, symmetrized, hermitian matrix

$$\tilde{\epsilon}_{\mathbf{G},\mathbf{G}'}(\mathbf{q},\omega) \equiv \frac{|\mathbf{q}+\mathbf{G}|}{|\mathbf{q}+\mathbf{G}'|}\epsilon_{\mathbf{G},\mathbf{G}'}(\mathbf{q},\omega) = \tilde{\epsilon}^*_{\mathbf{G}',\mathbf{G}}(\mathbf{q},\omega)$$

[6] Whereas our ansatz in Sec. 1.1 is $K = 1/\epsilon = 1/(1-U\Pi)$ — in shorthand notation for the bare Coulomb interaction U and the *irreducible* polarizability Π — Ref. [74] starts from the same $K = 1+U\hat{\Pi}$ with the *full* polarizability $\hat{\Pi}$. This seems to avoid a matrix inversion to obtain K, but unfortunately the calculation of $\hat{\Pi}$ requires the knowledge of the excited states ($|n\rangle$ and ω_n there), whereas knowledge of the ground state spectrum ($|\nu\mathbf{k}\rangle$ and $E_{\nu\mathbf{k}}$ here) suffices to calculate Π. Note that our $K_{\mathbf{G},\mathbf{G}'}$ cannot be computed by just switching the $-$-sign in our Eq. (4) to $+$, because we encounter susceptibilities of magnitude $\sim$ 1–10.

also is in the literature [68–70,75–79]. [7] The form contains the same information as $\epsilon_{\mathbf{G},\mathbf{G}'}$. The multiplication of the rows and columns of the matrix can be "undone" by divisions of the columns and rows of the inverse:

$$\tilde{K}_{\mathbf{G},\mathbf{G}'}(\mathbf{q},\omega) \equiv \frac{|\mathbf{q}+\mathbf{G}|}{|\mathbf{q}+\mathbf{G}'|} K_{\mathbf{G},\mathbf{G}'}(\mathbf{q},\omega).$$

$\tilde{\epsilon}_{\mathbf{G},\mathbf{G}'}$ is mainly employed to deal technically with singularities as $\mathbf{q} \to 0$ [5], to define photonic band-structures, or when the dielectric response is defined in terms of vector fields instead of potentials. The familiar energy term of DFT couples electrons to the longitudinal, scalar potential (see Sect. 1.5.1), and consequently this part of the literature favors the use of ϵ.

1.5 Implementation

1.5.1 DFT Input

As noted, we take the Bloch functions $|\nu\mathbf{k}\rangle$ as the KS orbital solutions from GTOFF. Those self-consistent solutions are expressed as a superposition of Hermite GTO's [80–83]

$$\begin{aligned}\psi_{\nu,\mathbf{k}}(\mathbf{r}) &\equiv \varphi_{\nu,\mathbf{k}}(\mathbf{r}) \\ &= \sum_{\mathbf{R}} \mathrm{e}^{\mathrm{i}\mathbf{k}\cdot\mathbf{R}} \sum_{b} c_{\nu\mathbf{k}b} N_{\mathbf{n}\alpha} g(\mathbf{n},\alpha,\mathbf{r}-\mathbf{R}-\mathbf{r}_b),\end{aligned} \tag{16}$$

with $\mathbf{R}$ the real-space lattice vectors, $N_{\mathbf{n}\alpha}$ normalization constants, $c_{\nu\mathbf{k}b}$ expansion coefficients for basis function b (including intra/inter-site contraction coefficients), $\mathbf{r}_b$ the centers of the GTO's relative to the origin of the unit cell, $g(\mathbf{n},\alpha,\mathbf{r}-\mathbf{R}-\mathbf{r}_b)$ primitive GTO's centered at sites $\mathbf{R}+\mathbf{r}_b$ with exponents α and types indicated by the triple indices $\mathbf{n}=(n_1,n_2,n_3)$.

In addition to the usual approximations of a finite basis set expansion, two other approximations are made. Explicitly (16) presumes that the KS Bloch states are reasonable approximations to the proper quasi-particle Bloch states (see above). Implicitly there is the use of the associated KS eigenvalues in the energy denominator of Eq. (7). At least the procedure is well-defined and can be improved upon in various ways, ranging upward in sophistication from simple scissors operators [84–87]. The static response $\Pi(\mathbf{q}+\mathbf{G},\mathbf{q}+\mathbf{G}',\omega=0)$ is a ground state property, though, and accessible to the time-independent KS procedure. This is an ultimate consequence of the fact that the energy term associated with (5) couples the external potential to the electron *density*. (That

[7] An $\hat{e}$ is missing in front of $(\vec{q}+\vec{G})$ in (4.7) of [77].

means the interaction with transverse fields — the vector potential in the kinetic energy operator — is neglected. In dipole order this additional term contains polarization operators that create and destroy *electron-hole pairs* and are *not* diagonal in the band indices [88–91]. It also means that the Maxwell field is not quantized, not retarded, etc.) Some cancellation of errors [92] of these two approximations seems to ensure that the eigenspectrum and eigenvalues of the "diagonalized," non-interacting KS "particles," integrated over the occupied *and* unoccupied states, represent the ground state exactly. Closely related manifestations of this phenomenon are the sum rules related to the electron density (Sec. 2.2) and methods to calculate the ω-dependent dielectric function from knowledge of the occupied parts of the band-structure alone [93].

The random phase approximation [94,95] formally is the lowest order (the non-interacting) term in a perturbative expansion of the effective interaction in many-fermion systems. As we substitute the electrons and holes in this perturbative expansion by their KS counterparts, which are already "dressed" by some (static) approximation to their self-energy, the connection to the Dyson perturbation theory is broken. Higher orders of the irreducible polarization are at least well-defined [96,97], but they introduce self-energy and exchange diagrams which do not make sense if the (frequency-dependent) Green's function derived from Eq. (5) is inserted, which already encapsulates some of these aspects of itself. Responses to this problem are (i) turning towards the *GW* expansion in the original many-particle theory, where the auxiliary DFT delivers an approximation to the screened interaction W [6–9], (ii) computing within the DFT self-consistent *GW* solutions by iteration, (iii) re-interpreting Eq. (7) on the basis of the time-dependent density (current) functional theory, or (iv) repeating the perturbative analysis of [44] in the Kohn–Sham context. The comparison of Eqs. (3), (4) and (7) with the results of approach (iv) shows that our calculation misses the aspect of the exchange-correlation that is commonly expressed in terms of a local-field *factor* (as distinct from the local field *effects* of the umklapp-processes).

1.5.2 Wavenumber Representation

The transformation from GTO's to plane waves $u_{\nu,\mathbf{k},\mathbf{G}}$ proceeds efficiently via the FT of primitive Hermite GTO's, expressible in closed form as [98]

$$\int \mathrm{e}^{-\mathrm{i}\mathbf{q}\cdot\mathbf{r}}\, g(\mathbf{n},\alpha,\mathbf{r})\,\mathrm{d}^3 r = \left(\frac{\pi}{\alpha}\right)^{3/2} \mathrm{e}^{-q^2/(4\alpha)} \prod_{l=1}^{3} (-\mathrm{i}q_l)^{n_l}.$$

(The FT is proportional to a Cartesian GTO in reciprocal space. This is a strict consequence of the fact that the FT of Cartesian GTO's are Hermite GTO's and vice versa [99,100].) Only this infinite integral is required, because the combination of the integral over the UC (8) with the sum over lattice vectors

(16) removes the individual shape of the unit cell from the computation of $u_{\nu\mathbf{k},\mathbf{G}}$. The equivalence of both representations is maintained by monitoring the accumulated norm for each $|\nu,\mathbf{k}\rangle$ relative to the exact values,

$$\sum_{\mathbf{G}} |u_{\nu,\mathbf{k},\mathbf{G}}|^2 = V_{\mathrm{UC}} \tag{17}$$

related to the norm of the real-space representations

$$\int_{\mathrm{UC}} |\varphi_{\nu,\mathbf{k}}(\mathbf{r})|^2 \, \mathrm{d}^3 r = 1$$

by Parseval's theorem.

Note that the current implementation did not relax and improve the band structure by computing the self-consistent field (diagonalizing the KS Hamiltonian) with the larger PW basis, which would result in new energies $E_{\nu\mathbf{k}}$ and states $\varphi_{\nu,\mathbf{k}}$ above and below E_{F}, but be most beneficial to the higher-lying unoccupied bands.

1.5.3 Linear Analytical Tetrahedron Method

Integration (summation) over BZ's via some form of the Linear Analytical Tetrahedron Method, the three-dimensional generalization of the trapezoidal rule, is well-known in solid and surface electronic structure calculations [2,101–107]. However, the specific implementation is significant in the context of heavy computational demands. We subdivide the integration region of the integral (7) into parallelepipeds, then subdivide each of those into six tetrahedra. Recursive further subdivision of a given tetrahedron into smaller tetrahedra is done if one or both Fermi functions run through it. Next comes linearization of the product of the matrix elements in the numerator and of the energy denominator — the later being crucial [105,106] but sometimes ignored [54,55] — inside each tetrahedron for each ω. We expect linearization of the numerator — as in Ref. [2,78,108] — to yield results of higher quality than the less expensive approximation by a constant, mean matrix element in each tetrahedron, which is found in the literature as well [101–104]. Finally, the resulting approximated integral is evaluated analytically after an affine coordinate transformation into the unit tetrahedron.

The contribution generated by the term $i\eta$ in the denominator of Eq. (7) ("real transitions") is, in the coordinate system of the unit tetrahedron, proportional to

$$\int_0^1 \mathrm{d}r_1 \int_0^{1-r_1} \mathrm{d}r_2 \int_0^{1-r_1-r_2} \mathrm{d}r_3$$
$$\times \left[c_1 + (c_2 - c_1)r_1 + (c_3 - c_1)r_2 + (c_4 - c_1)r_3\right]$$
$$\times \delta\left(V_1 + (V_2 - V_1)r_1 + (V_3 - V_1)r_2 + (V_4 - V_1)r_3\right)$$
$$= \frac{1}{V_4 - V_1} \int_0^1 \mathrm{d}r_1 \int_0^{r_m} \mathrm{d}r_2 (T_0 + T_1 r_1 + T_2 r_2); \tag{18}$$

with

$$T_0 \equiv c_1 - (c_4 - c_1)\frac{V_1}{V_4 - V_1},$$
$$T_i \equiv c_{i+1} - c_1 - (c_4 - c_1)\frac{V_{i+1} - V_1}{V_4 - V_1} \quad (i = 1, 2),$$
$$r_m \equiv \max\left[1 - r_1, -\frac{V_1 + (V_2 - V_1)r_1}{V_3 - V_1}, \frac{V_4 - (V_4 - V_2)r_1}{V_4 - V_3}\right].$$

Here the polynomial with the coefficients c_i is the matrix element product $m^*_{\mathbf{G}} m_{\mathbf{G}'}$ at a general point inside the unit tetrahedron, c_1 is the product evaluated at the vertex mapped to the origin, and similarly V_1 is the energy denominator $\hbar\omega + E_{\nu\mathbf{k}} - E_{\nu'\mathbf{k}+\mathbf{q}}$ evaluated at that vertex. The remaining c_i are the matrix element products at the i-th vertex and similarly for the V_i. The resulting integrals (18) of linear functions over trapezoids [pieces of the unit triangle $0 \le r_1 \le 1$, $0 \le r_2 \le 1 - r_1$, depending on the points of intersection of the three straight lines that define r_m] have simple analytical solutions. The full integral (7) is then extracted efficiently from this intermediate result by a numerical Kramers–Kronig (Hilbert) transformation. Technical details are in App. D.

A disadvantage of the tetrahedron method is the perturbation of the symmetry (12) by the division of reciprocal space into tetrahedra that are not necessarily mapped onto each other by the point group operations. (A two-dimensional example of our implementation with common alignment of the tetrahedra is Fig. 1(c) in Ref. [109].) This source of noise can be controlled (i) by reducing the order of the assumed point group, which turns out to build statistical averages over sets $O\mathbf{q}$ of equivalent points covered by non-equivalent tetrahedra, and (ii) by increasing the density of the $\mathbf{k}$-mesh.

Note that weights of $\mathbf{k}$-points are not used or defined in this scheme to calculate Eq. (7) for two reasons:

- The concept of star weights (multiplicities) does not apply, because the integrand does not have the familiar point symmetries comparable to Eq. (10) or Eq. (11) as a function of $\mathbf{k}$ for fixed (but non-zero) $\mathbf{q}$, $\mathbf{G}$ and $\mathbf{G}'$,

which are needed to reduce BZ integrals of one-particle properties similar to the density of states to the IBZ.
- Eq. (18) cannot be decomposed into a sum of terms without mixing c_i and V_i of different vertex indices i in these terms. This fails even if the c_i are further approximated by constants in the tetrahedra, but would be an indispensable first step to introduction of **k**-weights.

This distinction between integrands which are local and non-local in **k**, and not singularities in Eq. (7) as asserted by Farid *et al.* [110], is the reason that "special point" methods are not available for general **q**.

1.6 Integrating the Energy Loss Function

The product $|\mathbf{q}+\mathbf{G}|^2\epsilon_{\mathbf{G},\mathbf{G}'}(\mathbf{q},\omega)$ is calculated and, in compensation, the term q^2 in the denominator of Eq. (2) and the term $|\mathbf{q}+\mathbf{G}|^2$ in the denominator of Eq. (1) are dropped (cancellation of divergences). The dielectric function is tabulated for **q** commensurate with the uniform mesh of wave vectors used in the underlying GTOFF calculation but covering higher BZ's as well as the first. $\operatorname{Im} K_{\mathbf{G},\mathbf{G}'}$ is linearized inside each **q**-space tetrahedron. Multiplied by the linear factor $\mathbf{q}\cdot\mathbf{v}$, the integrals (2) over tetrahedra are done analytically, then summed up. In a notation similar to Eq. (18) they are proportional to

$$\begin{aligned}
&\int_0^1 \mathrm{d}r_1 \int_0^{1-r_1} \mathrm{d}r_2 \int_0^{1-r_1-r_2} \mathrm{d}r_3 \\
&\times [p_1 + (p_2-p_1)r_1 + (p_3-p_1)r_2 + (p_4-p_1)r_3] \\
&\times [d_1 + (d_2-d_1)r_1 + (d_3-d_1)r_2 + (d_4-d_1)r_3] \\
&= \frac{1}{120}\left[\sum_{i=1}^4 p_i \sum_{j=1}^4 d_j + \sum_{i=1}^4 p_i d_i\right],
\end{aligned}$$

where p_i and d_i are the values of $\mathbf{v}\cdot\mathbf{q}$ and $\operatorname{Im} K_{\mathbf{0},\mathbf{0}}(\mathbf{q},\mathbf{q}\cdot\mathbf{v})/q^2$ at the four vertices of the tetrahedron.

Evaluation of Eq. (2) involves a region of integration which covers the half-infinite "triangle"

$$0 \le \omega \le \mathbf{v}\cdot\mathbf{q} \tag{19}$$

of combined energy and momentum transfers. Values outside the $(\mathbf{q},\omega)$-meshes are replaced by the vacuum response, $\epsilon_{\mathbf{G},\mathbf{G}'}(\mathbf{q},\omega) = \delta_{\mathbf{G},\mathbf{G}'}$.

2 Hexagonal Bulk Lithium

To illustrate the physics which emerges we study crystalline Li in the hcp phase.

2.1 Structure

The hexagonal, close packed form of solid lithium is most probably the stable form at zero temperature, if more complicated close-packed structures are left aside [111–120]. [8] However the KS band structure for equilibrium hcp Li apparently has not been published, whereas the cubic modifications are well studied [121–129], hence see Figs. 1–2. These band energies and the associated KS orbitals are the inputs to the results which follow. The KS basis 41111/111/11, 5s3p2d, is a partially de-contracted set of the "interior" layer set in Ref. [130], augmented by two d-type GTO's with $\alpha = 0.36/a_0^2$ and $0.14/a_0^2$ taken from Ref. [3]. d-type "polarization" functions are essential to avoid a spurious band-gap ≈ 20 eV above $E_{\rm F}$, as is known from more detailed partitioning of the density of states [131]. The expectation value of the kinetic energy operator is $3\alpha E_0/a_0^2$ for s-type, $5\alpha E_0/a_0^2$ for p-type, and $7\alpha E_0/a_0^2$ for d-type isolated GTO's, which provides estimates of which energy region is dominated by which exponent. (E_0 is 1 rydberg.) Adding the d orbitals lowers the ground state energy by 45 meV/atom [132] [9] and lifts a KS state at Γ from -0.1 eV to the Fermi surface.

Each $\varphi_{\nu,\mathbf{k}}(\mathbf{r})$ was mapped to 785 plane waves, all those with $|\mathbf{G}| < 5.7/a_0$. The norm (17) was above $0.965V_{\rm UC}$ for all states in the two bands of K electrons, and above $0.992V_{\rm UC}$ for all other bands touched, high above the Fermi surface.

Cross sections through the all-electron momentum density (EMD) (without corrections [133–136])

$$\rho(\mathbf{k}+\mathbf{G}) \equiv \frac{1}{V_{\rm UC}} \sum_{\nu} f_{\nu,\mathbf{k}} |u_{\nu,\mathbf{k},\mathbf{G}}|^2$$

are shown in Figs. 3–4 as a function of $\mathbf{k}+\mathbf{G}$. (All EMD's shown are cross sections through the distributions, not "projected" on the momentum planes by integrating over the remaining third, perpendicular direction.) The EMD

[8] The reference to the work by Boettger and Trickey in Table I of [119] is misleading, because the hcp form was not considered by the latter authors.

[9] This energy drop is close to ~ 50 meV per atom reported by Knittle et al. [132] upon adding d-orbitals to the localized basis of cubic BN, but much more than in [188] upon adding one tighter d-orbital in graphite.

provides an elementary check that the conversion to the PW basis is correct. It also gives a first idea of the importance of umklapp-processes: because the product of matrix elements in Eq. (7) correlates $|\nu\mathbf{k}\rangle$ with $|\nu\mathbf{k}+\mathbf{G}-\mathbf{G}'\rangle$ indirectly through unoccupied states $|\nu'\mathbf{k}+\mathbf{q}\rangle$, the product of matrix elements $m^*_{\mathbf{G}} m_{\mathbf{G}'}$ remains small for $\mathbf{G} \neq \mathbf{G}'$ if the EMD is in essence concentrated inside the first BZ. In this admittedly over-simplified interpretation, the EMD points at constraints on "horizontal" correlations in the band-structure of the extended zone scheme, akin to the way in which the joint density of states provides an estimate of the available "vertical" overlaps.

Eqs. (10) and (11) mean that the EMD has the symmetry of the isogonal point group of the crystal, plus (if missing therein) the inversion symmetry. The EMD as a function of $\mathbf{k}+\mathbf{G}$ has this feature in common with the energy loss as a function of $\mathbf{v}$ evaluated by Eq. (2). The 6-fold axis in Fig. 3 combines, for example, the C_{3z} symmetry of the crystal field with the inversion. If the sum over bands ν is restricted to the two bands with core electrons, this 6-fold symmetry becomes nearly circular.

2.2 Dielectric Matrix

The influence of the local field effects (LFE's), i.e., of the "wing" (one of $\{\mathbf{G},\mathbf{G}'\}$ non-zero) and "body" (both $\mathbf{G}$ and $\mathbf{G}'$ non-zero) matrix elements remains small for lithium. Figures 5–6 show for comparison $\operatorname{Im}\epsilon_{\mathbf{G},\mathbf{G}'}(\mathbf{q},\omega)$ of the "head" element $\mathbf{G}=\mathbf{G}'=\mathbf{0}$ and of the "body" element $\mathbf{G}=\mathbf{G}'=(0001)$. Values above 45 eV include excitations from the Li K-shell, the lowest band in the band-structure, which inevitably are missing in pseudopotential calculations [121–123]. LFE's are not included in Fig. 7, which shows $\operatorname{Im}(1/\epsilon_{\mathbf{0},\mathbf{0}})$ instead of $\operatorname{Im} K_{\mathbf{0},\mathbf{0}}$.

The computed dielectric function of Figs. 5 and 7 satisfies the sum rules [77,137–146] [10] [11] [12] [13]

$$\int_0^\infty \omega\ \operatorname{Im}\epsilon_{\mathbf{G},\mathbf{G}}(\mathbf{q},\omega)\,\mathrm{d}\omega = -\int_0^\infty \omega\ \operatorname{Im} K_{\mathbf{G},\mathbf{G}}(\mathbf{q},\omega)\,\mathrm{d}\omega = \frac{\pi}{2}\omega_p^2 \tag{20}$$

[10] for sum rules with pseudopotentials see [143]

[11] for nonlocal potentials see [87], for nonlinear sum rules [144].

[12] For intricacies by a scissors operator, see Ref. [145].

[13] As shown by Taut [137,138], our combination of the RPA and the KK formulas (App. D) ensures that the first two expressions in Eq. (20) are the same — even if they are not equal to the third, last, due to basis set incompleteness. If the system supports undamped plasmons, their contribution to the sum rule for $\operatorname{Im}(1/\epsilon)$ is obtainable from the slope $\partial \operatorname{Re}\epsilon(\mathbf{q},\omega)/\partial\omega$ at the plasmon line $\epsilon(\mathbf{q},\omega)=0$, see for example [146].

of the diagonal elements $\epsilon_{\mathbf{G},\mathbf{G}}(\mathbf{q},\omega)$ and $K_{\mathbf{G},\mathbf{G}}(\mathbf{q},\omega)$ within 9%, if the integration of the energy-spectrum is restricted to frequencies below the threshold of K-shell excitations, and if the result is compared with the squared plasmon frequency

$$\omega_p^2 \equiv ne^2/(\epsilon_0 m)$$

of the conduction electrons with mean density $n = 2/V_{\mathrm{UC}}$. A test on the all-electron sum rule with $n = 6/V_{\mathrm{UC}}$ shows that for $\hbar\omega < 60$ eV only about 60% of the density is recovered, and the integral (20) still is growing distinctly as a function of the upper limit of the integration. We observe the decrease of the first moment of $\mathrm{Im}\,\epsilon_{\mathbf{0},\mathbf{0}}(\mathbf{q},\omega)$ as function of $\mathbf{q}$ that is known from atomic targets [53,147], a closer compliance with the sum rule if the KS basis is enlarged, and — even for much simpler model calculations — an overshooting for small $\mathbf{q}$ as reported for solid and atomic aluminum [148,149].

2.3 Computed Electronic Energy Loss

The energy loss cross sections shown in Fig. 8 are based on a coarser GTOFF grid with $6 \times 6 \times 4$ points in the BZ (21 points in the IBZ), using only the $\mathbf{G} = \mathbf{G}' = \mathbf{0}$ element of the dielectric matrix. An oscillatory behavior of $S(\mathbf{v})$ for $v \gtrapprox v_0$ is an unmistakable indication that some values of the energy loss function $\mathrm{Im}\,K_{\mathbf{0},\mathbf{0}}(\mathbf{q},\omega)$ have already been replaced by zeros for some ω larger than the tabulated maximum. [The required range becomes larger and larger for increasing $\mathbf{v}$; see Eq. (19).] The agreement with the experimental results by Eppacher *et al.* in the synopsis of Fig. 9 is quite satisfactory but also somewhat deceptive, because (partially cancelling) corrections for the nonlinear dielectric response [150] (i.e., the Barkas effect) and for transient electron capture by the protons are missing in our calculation. (Partial cancellation means that the Barkas term generally increases S, whereas the time-averaged, temporarily neutralized, actual ion ought to display a decreased S compared with the theoretical, bare ion — effects like antiscreening [151] left aside.)

The calculation by Grande and Schiwietz [152] is not included in Fig. 9, because it includes only excitations within the conduction band, which drastically reduces the applicability of the results to velocities below their maximum, $S \approx 1$ eVcm^2/10^{15} atoms at $v \approx 0.2v_0$.

Under compression to $a = 5.36a_0$ and $c = 8.79a_0$, reducing the lattice constants by 5% and V_{UC} by 15%, the maximum of the stopping cross section decreases by about 5–10%. The error bars and scattering in the results are too large to pick out a corresponding shift on the v-axis. The negative correlation of the stopping cross section (per target electron) with the density is

the familiar gas-solid effect and also is found in the homogeneous electron gas model. Comparing the aforementioned percentages, $\mathrm{d}E/\,\mathrm{d}x \propto S/V_{\mathrm{UC}}$ remains positively correlated with the density; as expected, the range of ions is shorter in more compact targets.

Gapless (metallic) dielectric functions [15–17,60,61], a kinetic theory without lower limits of the transferable energy [153], and the results of the inverse scattering theory [154–158] predict a linear rise $\mathrm{d}E/\,\mathrm{d}x \propto v$ at small v, but experiments [159–162] and more detailed theories [163–168] indicate more complicated dependencies. Fig. 10 sketches a one-band, homogeneous model material with occupied states at the origin, no free states ($\mathrm{Im}\,1/\epsilon(\omega, q) = 0$) in the range up to a gap $\hbar\omega_g$, and the dispersion $\hbar\omega = \hbar^2k^2/(2m)$ above this "ionization" threshold (a simplified Bethe ridge [169–171]). The integral (2) becomes an integral over $\omega \leq qv$ in this model, because the integration over the polar and azimuthal angles between $\mathbf{q}$ and $\mathbf{v}$ can be performed analytically [10]. It remains zero if

$$v < v_0\sqrt{\hbar\omega_g/E_0}/2, \tag{21}$$

where E_0 is one rydberg. Fig. 11 is the corresponding numerical result for lithium, if Π is calculated with K-shell excitations alone. The formula predicts a threshold velocity of $0.9v_0$ for $\hbar\omega_g = 45$ eV, which is close to what is seen in the figure as the onset of the electronic energy loss. The formula predicts threshold ion energies of 6 keV/u and 2 keV/u for $\hbar\omega_g = 14$ eV and 4 eV. In accordance with the measurement by Eder *et al.* [172], the threshold is not observed at proton energies above 2 keV if the band gap is as low as 4 eV.

Note that, while showing this result of an incomplete summation over band transitions, we do *not* imply that S in the multi-band RPA may be generally rewritten as a sum of contributions of individual bands, in contrast to a Hartree–Fock formulation by Dettmann [74,171], our Orbital Local Plasma decomposition of the Bethe theory [173–175] or the original Kaneko ansatz [163]. This explains why Fig. 8 is not a sum of a smooth curve (due to valence-band excitations) plus the more scattered data of the K-shell excitations of Fig. 11. For example, the vertical order of data points at a given velocity v is not preserved when switching between those two figures.

Acknowledgements

Support by grant DAA-H04-95-1-0326 from the U.S. Army Research Office is gratefully acknowledged.

A Energy Loss of Probes with Frozen Charge Distributions

Demonstration of Eq. (1) requires redoing a number of familiar arguments for punctiform ions. The energy transfer per unit time from a charge distribution $\rho_{\mathrm{ext}}(\mathbf{r},t)$ to a dielectric target in classical electrodynamics is

$$\frac{\mathrm{d}E}{\mathrm{d}t} = \int \rho_{\mathrm{ext}}(\mathbf{r},t)\mathbf{v}\cdot\mathbf{E}_{\mathrm{ind}}(\mathbf{r},t)\,\mathrm{d}^3r < 0. \tag{A.1}$$

The differential $\mathrm{d}t$ corresponds to an arbitrarily short time interval within which the ion nucleus moves by $\mathrm{d}x = v\,\mathrm{d}t$. This microscopic definition used in the dielectric theory of electronic energy loss is clearly different from conceptualizations based on differentials of the target thickness [176]. The concept of target thicknesses would only be applicable to targets with planar geometry and breaks down for thicknesses on the (sub)monolayer scale. The relationship (A.1) establishes a microscopic theory because (i) it means a Hartree approximation to the interaction between the charges ρ_{ext} and those that create $\mathbf{E}_{\mathrm{ind}}$ [177], and (ii) the ion nucleus is treated classically along a classical trajectory. With these assumptions, no energy-time uncertainty relation hinders the definition of the differential quotient $\mathrm{d}E/\mathrm{d}t$ as the limit of a quotient of finite differences for *any* target geometry.

In Fourier space, neglecting the interaction of the ion with transverse components of the fields, the electrical field of the induced polarization in terms of its "wake" potential reads [14]

$$\mathbf{E}_{\mathrm{ind}}(\mathbf{q},\omega) = -\mathrm{i}\mathbf{q}\Phi_{\mathrm{ind}}(\mathbf{q},\omega). \tag{A.2}$$

Any wave vector $\mathbf{q}$ of the external field induces a discrete spectrum of polarizations at wave vectors $\mathbf{q}+\mathbf{G}$ in a crystal. Their components are linked by the elements of the inverse dielectric matrix $K_{\mathbf{G},\mathbf{G}'}$ [44]

$$\Phi_{\mathrm{ind}}(\mathbf{q}+\mathbf{G},\omega) = \left[K_{\mathbf{G},\mathbf{0}}(\mathbf{q},\omega) - \delta_{\mathbf{G},\mathbf{0}}\right]\Phi_{\mathrm{ext}}(\mathbf{q},\omega),$$

which is used here in the formulation

$$\begin{aligned}\Phi_{\mathrm{ind}}(\mathbf{q},\omega) &= \sum_{\mathbf{G}}\left[K_{\mathbf{G},\mathbf{0}}(\mathbf{q}-\mathbf{G},\omega) - \delta_{\mathbf{G},\mathbf{0}}\right]\Phi_{\mathrm{ext}}(\mathbf{q}-\mathbf{G},\omega)\\ &= \sum_{\mathbf{G}}\left[K_{\mathbf{0},\mathbf{G}}(\mathbf{q},\omega) - \delta_{\mathbf{G},\mathbf{0}}\right]\Phi_{\mathrm{ext}}(\mathbf{q}+\mathbf{G},\omega).\end{aligned}$$

[14] The sign convention in the exponent of Fourier transforms is different for example in Refs. [46,69]. This would switch a sign here, in the Kramers–Kronig formulas, and in other frequency and wavenumber dependent formulas, like Eqs. (2) and (A.2).

Fields and potentials are eliminated from the right hand side of Eq. (A.1) via the Poisson equation

$$\Phi_{\rm ext}(\mathbf{q},\omega) = \rho_{\rm ext}(\mathbf{q},\omega)/(\epsilon_0 q^2).$$

Assuming a constant velocity $\mathbf{v}$, a straight path through the origin of coordinates, and a frozen $\rho_{\rm ext}$,

$$\begin{aligned}\rho_{\rm ext}(\mathbf{r},t) &= \rho_{\rm ext}(\mathbf{r}-\mathbf{v}t),\\ \rho_{\rm ext}(\mathbf{q},\omega) &= 2\pi\delta(\omega-\mathbf{q}\cdot\mathbf{v})\rho_{\rm ext}(\mathbf{q}),\end{aligned}$$

splits off the ion form factor (the spatial Fourier transform of the charge distribution) $\rho_{\rm ext}(\mathbf{q}) = \rho^*_{\rm ext}(-\mathbf{q})$ [12–14]. Gathering terms yields

$$\begin{aligned}\frac{{\rm d}E}{{\rm d}t} = \frac{\rm i}{\epsilon_0}\int\frac{{\rm d}^3q}{(2\pi)^3}\rho_{\rm ext}(\mathbf{q})\mathbf{v}\cdot\mathbf{q}\sum_{\mathbf{G}}{\rm e}^{-{\rm i}\mathbf{G}\cdot\mathbf{v}t}\,\frac{\rho^*_{\rm ext}(\mathbf{q}-\mathbf{G})}{(\mathbf{q}-\mathbf{G})^2}\\ \times\int_{-\infty}^{\infty}{\rm d}\omega\,[K_{\mathbf{0},\mathbf{G}}(-\mathbf{q},\omega)-\delta_{\mathbf{G},\mathbf{0}}]\,\delta\left(\omega+(\mathbf{q}-\mathbf{G})\cdot\mathbf{v}\right).\end{aligned}\tag{A.3}$$

Terms $\propto \exp({\rm i}\mathbf{G}\cdot\mathbf{v}t)$ deliver a net contribution only if they are not rapidly oscillatory, i.e., in the cases $\mathbf{G}\perp\mathbf{v}$. (The energy loss by the associated bremsstrahlung hence is ignored [73].) In addition we use the analogue of Eq. (14) to obtain

$$\begin{aligned}\frac{{\rm d}E}{{\rm d}x} = \frac{\rm i}{\epsilon_0 v}\int\frac{{\rm d}^3q}{(2\pi)^3}\rho_{\rm ext}(\mathbf{q})\mathbf{v}\cdot\mathbf{q}\sum_{\mathbf{G}\perp\mathbf{v}}\frac{\rho^*_{\rm ext}(\mathbf{q}+\mathbf{G})}{(\mathbf{q}+\mathbf{G})^2}\\ \times\int_{-\infty}^{\infty}{\rm d}\omega\left[K^*_{\mathbf{0},\mathbf{G}}(\mathbf{q},\omega)-\delta_{\mathbf{G},\mathbf{0}}\right]\delta\left(\omega-\mathbf{q}\cdot\mathbf{v}\right).\end{aligned}\tag{A.4}$$

The values at negative ω can be eliminated using what follows from Eqs. (3) and (14),

$$K_{\mathbf{G},\mathbf{G}'}(\mathbf{q},\omega) = K^*_{-\mathbf{G},-\mathbf{G}'}(-\mathbf{q},-\omega),$$

and simultaneously reversing the signs of ω, $\mathbf{q}$ and $\mathbf{G}$:

$$\begin{aligned}\int{\rm d}^3q\,\rho_{\rm ext}(\mathbf{q})\mathbf{v}\cdot\mathbf{q}\sum_{\mathbf{G}\perp\mathbf{v}}\frac{\rho^*_{\rm ext}(\mathbf{q}+\mathbf{G})}{|\mathbf{q}+\mathbf{G}|^2}\\ \times\int_{-\infty}^{0}{\rm d}\omega\left[K^*_{\mathbf{0},\mathbf{G}}(\mathbf{q},\omega)-\delta_{\mathbf{G},\mathbf{0}}\right]\delta\left(\omega-\mathbf{q}\cdot\mathbf{v}\right)\end{aligned}$$

$$= -\int \mathrm{d}^3q\, \rho^*_{\mathrm{ext}}(\mathbf{q})\mathbf{v}\cdot\mathbf{q} \sum_{\mathbf{G}\perp\mathbf{v}} \frac{\rho_{\mathrm{ext}}(\mathbf{q}+\mathbf{G})}{|\mathbf{q}+\mathbf{G}|^2}$$
$$\times \int_0^\infty \mathrm{d}\omega \left[K_{\mathbf{0},\mathbf{G}}(\mathbf{q},\omega) - \delta_{\mathbf{G},\mathbf{0}}\right] \delta\left(\omega - \mathbf{q}\cdot\mathbf{v}\right).$$

Eq. (A.4) becomes

$$\frac{\mathrm{d}E}{\mathrm{d}x} = \frac{1}{4\pi^3\epsilon_0 v} \int \mathrm{d}^3q\, \mathbf{v}\cdot\mathbf{q} \int_0^\infty \mathrm{d}\omega \delta\left(\omega - \mathbf{q}\cdot\mathbf{v}\right)$$
$$\times \sum_{\mathbf{G}\perp\mathbf{v}} \frac{1}{(\mathbf{q}+\mathbf{G})^2} \mathrm{Im}\left[K_{\mathbf{0},\mathbf{G}}(\mathbf{q},\omega)\rho^*_{\mathrm{ext}}(\mathbf{q})\rho_{\mathrm{ext}}(\mathbf{q}+\mathbf{G})\right]. \qquad \text{(A.5)}$$

This is the expression given at the outset of the paper.

If the origin of coordinates is shifted to a new location $\mathbf{b}$, the ion passes the (new) origin at impact parameter $-\mathbf{b}$,

$$\rho_{\mathrm{ext}}(\mathbf{r},t) = \rho_{\mathrm{ext}}(\mathbf{r}-\mathbf{v}t+\mathbf{b}).$$

This multiplies $\rho_{\mathrm{ext}}(\mathbf{q},\omega)$, effectively the form factor $\rho_{\mathrm{ext}}(\mathbf{q})$, by $\mathrm{e}^{\mathrm{i}\mathbf{q}\cdot\mathbf{b}}$ according to the shift-theorem of Fourier analysis, and therefore the product of form factors in Eq. (A.5) by a total factor of $\mathrm{e}^{\mathrm{i}\mathbf{G}\cdot\mathbf{b}}$. At the same time $K_{\mathbf{0},\mathbf{G}}(\mathbf{q},\omega)$ is multiplied by $\mathrm{e}^{-\mathrm{i}\mathbf{G}\cdot\mathbf{b}}$ according to Eq. (15). Both factors cancel, and $\mathrm{d}E/\,\mathrm{d}x$ is demonstrated to be invariant under this Galilean transformation, which means it depends only on the ion trajectory *relative* to the unit cells.

This result generalizes previous work [65,73,74] to an "effective charge" theory for crystalline targets, which reduces to the Brandt–Kitagawa form for $\mathbf{G} = 0$, subject of course to known limitations [12–14,177]. Remarks:

- We did not split the wavenumber $\mathbf{q}$ of the external field into a component inside the first BZ plus a reciprocal lattice vector to emphasize that the external field and its wavenumber spectrum are completely independent from the lattice and not restricted to the first BZ. This means that our $\int \mathrm{d}^3q$ is equivalent to the integral-sum $\int_{\mathrm{BZ}} d\vec{q} \sum_G$ in Eq. (3.15) by Saslow and Reiter [65] [only the $\mathbf{G} = \mathbf{0}$ term of Eq. (A.5) is actually present in their (3.15)] and to the double sum $\sum_{\mathbf{q}}^{\mathrm{BZ}} \sum_{\mathbf{G}}$ of Eq. (1) in [178].
- For spherically symmetric $\rho_{\mathrm{ext}}(\mathbf{q})$ [i.e., spherically symmetric $\rho_{\mathrm{ext}}(\mathbf{r})$, for example bare ions] (13) puts the following constraint on the anisotropy (directional dependence) of the energy loss calculated via (A.5): in cases where the translational part $\mathbf{w}$ of the space group operation $\{O|\mathbf{w}\}$ is zero,

or in the macroscopic approximation $\mathbf{G} = 0$,

$$\frac{\mathrm{d}E}{\mathrm{d}x}(\mathbf{v}) = \frac{\mathrm{d}E}{\mathrm{d}x}(O\mathbf{v}).$$

- Eq. (A.5) simplifies to Eq. (2) for punctiform ions [$\rho_{\mathrm{ext}}(\mathbf{q}) = Z_1 e$] and if only the term $\mathbf{G} = 0$ is retained, i.e., if the microscopic local field of the dielectric response, which also determines the electronic stopping contribution to channeling, is ignored. (i) In the terminology of Sect. 2.2, Eq. (2) will include local field effects if $K_{\mathbf{0},\mathbf{0}}$ is obtained by matrix inversion of $\epsilon_{\mathbf{G},\mathbf{G}'}$ but not if approximated by $1/\epsilon_{\mathbf{0},\mathbf{0}}$. (ii) However, $\mathrm{d}E/\,\mathrm{d}x$ in Eq. (2) still depends on the direction of $\mathbf{v}$ and is not strictly a "random" stopping power.

B Atomic Stopping Cross Sections

We quote results in terms of S and not in terms of $\mathrm{d}E/\,\mathrm{d}x$ in conformance with standard habits. However:

- From a tutorial point of view this is distracting, because the *atomic* number density N_2 is a hidden variable of the *electronic* energy loss (as opposed to the *nuclear* energy loss). Electronic stopping is — in the frozen phonon approximation of the target nuclei — a function of the *electronic* coordinates. Given the information of the band-structure, we actually calculate $\mathrm{d}E/\,\mathrm{d}x$ without using N_2.
- The important model of the free electron gas leaves N_2 undefined. Considering the stopping cross section per target *electron* would be more reasonable.
- For infinitely extended, periodic bulk targets, Eq. (9) establishes a 1-to-1 correspondence between S and $\mathrm{d}E/\,\mathrm{d}x$. [A mesoscopic average must be calculated by integrating $\mathrm{d}E/\,\mathrm{d}x$ over a distance covering an integer multiple of lattice vectors, since the microscopic information is not available in S. The integrated energy loss ΔE is a difference of ion energies measured at two places $\mathbf{r}$ that are an integer multiple of lattice vectors apart. Actually, the removal of the microscopic oscillatory changes is done when Eq. (A.3) is simplified to Eq. (A.4).] Calculations for thin layered targets [179–181] are faced with a fuzzy definition of the number density N_2, because the fringes of the electron density into the vacuum prohibit an unambiguous definition of their thickness, and because surface reconstruction plays a role. (The simplest model of surface reconstruction is a variable inter-layer spacing of atomic planes.) For these lower dimensional targets, $\mathrm{d}E/\,\mathrm{d}x$ remains explicitly $\mathbf{r}$-dependent even after the averaging over the microscopic length scales, noting that the exponent $\mathbf{v}t$ in Eq. (A.3) may be interpreted as $\mathbf{r}$: $\mathrm{d}E/\,\mathrm{d}x$ is non-zero during the passage through the target, but zero in the vacuum regions. The cumulative energy loss $\Delta E = \int \mathrm{d}E$ of a complete passage re-

mains well-defined. [15] In the case of two-dimensional crystalline targets, the product $N_2\,\mathrm{d}x$ in Eq. (9) has to be interpreted as an integrated whole, the areal number density of the target atoms, and S is the quotient of two well-defined quantities, the cumulative energy loss and the areal number density [182].

Similar remarks hold for a related pair of quantities, the generalized oscillator strength and the susceptibility.

- In heteronuclear targets, S is subject to a rather artificial averaging procedure [183,184] and leads to an analysis of the electronic stopping in terms of isolated atoms. The inherent limitation of this "Bragg-rule" ansatz is comparable to an attempt to obtain the band-structure of a compound material by an overlay of the dispersions of the homonuclear non-interacting subsets of atoms — with some adjustment of the Fermi energies, which only works for the non-overlapping core states. Only in the limit of high velocities $\mathrm{d}E/\,\mathrm{d}x$ approximately is a sum of contributions of independent "binary" collisions between the ion and the target atoms.
- Even in our Orbital Local Plasma Approximation for heteronuclear targets [174,175], where the underlying Bloch theory is expected to deliver an "atomic" description of the targets, the corresponding target atomic numbers Z_2 cancel eventually.

Starting from the bulk crystal (3D crystallinity), the stopping cross section of films (2D), wires (1D) and molecules (0D) are systematically obtained by an additional integration of $\mathrm{d}E/\,\mathrm{d}x$ over the coordinate along which the target is no longer periodic — integrations over one complete straight line for 2D, additional integrations over impact parameters for 1D and 0D — and replacing the volume number density N_2 by the areal number density, line number density and 1. By this construction, all (with respect to the translational symmetry) non-equivalent points in space are sampled by exactly one specific ion path out of an ensemble of trajectories; the targets with higher-dimensional crystallinity are special, unified cases of the targets with lower-dimensional crystallinity. For atoms and molecules, S is the familiar integrated differential cross section based on the impact-parameter dependent total energy loss of complete passages.

[15] The sum over $\mathbf{G}$ becomes an integral for those components of $\mathbf{G}$ that point into directions without periodicity, and infinitesimally small values of $\mathbf{G}\cdot\mathbf{v}$ appear in $\exp(\mathrm{i}\mathbf{G}\cdot\mathbf{v}t)$. This Fourier integral is nonzero even if $\mathbf{G} \not\perp \mathbf{v}$, i.e., the oscillatory behavior of the energy is no longer seen at finite, microscopic time scales, and the removal of these terms of the microscopic level in Eq. (A.3) is no longer feasible, because these terms now represent macroscopic length scales. In the limit of infinitely long edges of the unit cell of the superlattice, the ion meets the target molecule in a singular, non-recurring event.

C Inversion Symmetry in the BZ

Inversion symmetry (11) generally is used to reduce the size of the IBZ in DFT calculations, even if the inversion I is not an element of the isogonal point group of the real-space lattice. [This manipulation in $\mathbf{k}$-space is allowed because the complex-conjugation in Eq. (11) is another instance of rotations by complex "local" phase angles $\tau(\mathbf{k})$ in reciprocal space, which leave all relevant matrix elements invariant.]

- If I is *not* an element of the isogonal point group, the symmetry element $\{I|\mathbf{0}\}$ has virtually been added to the space group and does not necessarily commute with other elements $\{R|\mathbf{w}\}$ of the space group. Using [185, Eq. (1.5.12)]:

$$\{I|\mathbf{0}\}\{R|\mathbf{w}\} = \{IR|-\mathbf{w}\} \neq \{R|\mathbf{w}\}\{I|\mathbf{0}\} = \{IR|\mathbf{w}\}. \tag{C.1}$$

  One generally must use both R and I, Eqs. (10) and (11), to recover all points in the BZ from those in the IBZ, and the question may arise, whether the associated $\mathbf{w}$ in Eq. (10) has to be interpreted effectively as $-\mathbf{w}$ in this case. In fact, applying first Eq. (11) as part of the product $O \equiv RI = IR$ like

$$\begin{aligned} u_{O\mathbf{k},\mathbf{G}} = u^*_{R\mathbf{k},-\mathbf{G}} &= \left(\mathrm{e}^{-\mathrm{i}(-\mathbf{G})\cdot\mathbf{w}}\, u_{\mathbf{k},R^{-1}(-\mathbf{G})}\right)^* \\ &= \mathrm{e}^{-\mathrm{i}\mathbf{G}\cdot\mathbf{w}}\, u^*_{\mathbf{k},O^{-1}\mathbf{G}}, \end{aligned}$$

  or alternatively, in opposite order, first Eq. (10) like

$$\begin{aligned} u_{O\mathbf{k},\mathbf{G}} = \mathrm{e}^{-\mathrm{i}\mathbf{G}\cdot\mathbf{w}}\, u_{-\mathbf{k},R^{-1}\mathbf{G}} &= \mathrm{e}^{-\mathrm{i}\mathbf{G}\cdot\mathbf{w}}\, u^*_{\mathbf{k},-R^{-1}\mathbf{G}} \\ &= \mathrm{e}^{-\mathrm{i}\mathbf{G}\cdot\mathbf{w}}\, u^*_{\mathbf{k},O^{-1}\mathbf{G}} \end{aligned}$$

  yield the same, unambiguous result. Using the inversion symmetry in reciprocal space does not prevent the reconstruction of the phase of $u_{\nu,\mathbf{k},\mathbf{G}}$ of all $\mathbf{k} \in$ BZ.
- If $\{I|\mathbf{0}\}$ *is* an element of the space group, the closure property of the space group implies that Eq. (10) must be valid for products of the form (C.1),

$$\begin{aligned} u_{O\mathbf{k},\mathbf{G}} = u_{IR\mathbf{k},\mathbf{G}} = u_{R\mathbf{k},-\mathbf{G}} &= \mathrm{e}^{-\mathrm{i}\mathbf{G}\cdot\mathbf{w}}\, u_{\mathbf{k},-R^{-1}\mathbf{G}} \\ &= \mathrm{e}^{-\mathrm{i}\mathbf{G}\cdot\mathbf{w}}\, u_{\mathbf{k},O^{-1}\mathbf{G}}. \end{aligned}$$

  But the alternative application of Eq. (11) implies

$$u_{O\mathbf{k},\mathbf{G}} = u_{IR\mathbf{k},\mathbf{G}} = u^*_{R\mathbf{k},-\mathbf{G}} = \mathrm{e}^{\mathrm{i}\mathbf{G}\cdot\mathbf{w}}\, u^*_{\mathbf{k},O^{-1}\mathbf{G}},$$

  creating again a sign ambiguity of the form $\mathrm{e}^{\pm\mathrm{i}\mathbf{G}\cdot\mathbf{w}}$ after comparison with the foregoing equation. (The $u_{\nu,\mathbf{k},\mathbf{G}}$ can be chosen real-valued for lattices

with inversion symmetry.) An analysis based on the closure property, which is not detailed here, shows that in this case $\mathbf{w} = -\mathbf{w} + \mathbf{R}$ with some lattice vector $\mathbf{R}$, and therefore $\exp(\mathrm{i}\mathbf{G}\cdot\mathbf{w}) = \exp(-\mathrm{i}\mathbf{G}\cdot\mathbf{w})$, which resolves the ambiguity.

Though probably known in the case of PW codes, these things do not seem to be documented. They do not come into play as long as computations are limited to one-particle properties.

D Kramers–Kronig Analysis

The integrand of Eq. (7) has the form

$$\begin{aligned}\frac{M}{\hbar\omega - \Delta E + \mathrm{i}\eta} &= P\frac{M}{\hbar\omega - \Delta E} - \mathrm{i}\pi M\delta(\hbar\omega - \Delta E)\\ &\equiv H(\omega) + A(\omega),\end{aligned}$$

split into the "dispersive" contributions from "virtual" transitions H and the "absorptive" part from "real" transitions A. $A(\omega)$ and $H(\omega)$ are in general complex-valued [77]. P denotes the principal value, and M is the ω-independent product of matrix elements and the occupation numbers f. As shown by Johnson [77],

$$\frac{P}{\pi}\int_{-\infty}^{\infty}\frac{\mathrm{i}A(x)}{\omega - x}\,\mathrm{d}x = P\frac{M}{\hbar\omega - \Delta E} = H(\omega).$$

We divide by 2, add $A(\omega)/2$ on both sides, and use

$$\Theta(t) = \mathrm{i}\int_{-\infty}^{\infty}\frac{\mathrm{d}\omega}{2\pi}\frac{\mathrm{e}^{-\mathrm{i}\omega t}}{\omega + \mathrm{i}\eta}$$

to prove that

$$\begin{aligned}\frac{A(\omega) + H(\omega)}{2} &= \frac{P}{2\pi}\int_{-\infty}^{\infty}\frac{\mathrm{i}A(x)}{\omega - x}\,\mathrm{d}x + \frac{1}{2}A(\omega)\\ &= \int_{-\infty}^{\infty}\mathrm{e}^{\mathrm{i}\omega t}\,A(t)\Theta(t)\,\mathrm{d}t.\end{aligned}$$

Therefore, given just $A(\omega) = -A(-\omega)$, the full $A(\omega) + H(\omega)$ can be obtained via (i) Fourier Transform of $A(\omega)$ into the time domain, (ii) multiplication with and truncation by $2\Theta(t)$, then (iii) an inverse FT back into the frequency domain. In short, the Hilbert transformation is a convolution with $1/\omega$, expressible in the time domain as a multiplication that enforces causality [186,187]. Numerical instabilities from direct evaluation of the principal value do not arise; the analysis does not assume that $A(\omega)$, $H(\omega)$, $A(t)$ or $H(t)$ are real. This intermediate time representation has been used in analytical form as well [15–17].

The numerical workload in this Kramers–Kronig (KK) method is reduced by

(1) doing the KK transform only once for each ladder of ω values for a specific $(\mathbf{q}, \mathbf{G}, \mathbf{G}')$, not for each single tetrahedron, i.e., commuting the sum over band pairs and integral over the BZ with the integration inside the KK transform.
(2) avoiding the costly evaluations of the logarithms and the checks of the various sub-cases that demand Taylor expansions around removable singularities of the "virtual" transitions. Complementary to Eq. (18), these terms would be proportional to [78]

$$
\begin{aligned}
&P \int_0^1 \mathrm{d}r_1 \int_0^{1-r_1} \mathrm{d}r_2 \int_0^{1-r_1-r_2} \mathrm{d}r_3 \\
&\times \frac{c_1 + (c_2 - c_1)r_1 + (c_3 - c_1)r_2 + (c_4 - c_1)r_3}{V_1 + (V_2 - V_1)r_1 + (V_3 - V_1)r_2 + (V_4 - V_1)r_3} \\
&= c_1 \tilde{T}_1 + \sum_{j=2}^{4} (c_j - c_1)\tilde{T}_j,
\end{aligned}
$$

with

$$
\tilde{T}_1 \equiv \frac{1}{2} \sum_{j=1}^{3} \frac{V_j^2}{D_j} \ln \left| \frac{V_j}{V_4} \right|,
$$

$$
D_i \equiv \prod_{j=1, j\neq i}^{4} (V_i - V_j); \quad (i = 1, \ldots, 4),
$$

$$
\begin{aligned}
\tilde{T}_2 \equiv \frac{1}{6} \Big(&\frac{V_2^2}{D_2} - \frac{V_1^3 \ln(V_1/V_2)}{(V_2 - V_1)D_1} - \frac{V_3^3 \ln(V_3/V_2)}{(V_2 - V_3)D_3} \\
&- \frac{V_4^3 \ln(V_4/V_2)}{(V_2 - V_4)D_4} \Big),
\end{aligned}
$$

and $\tilde{T}_3$ and $\tilde{T}_4$ are defined by two consecutive circular shifts $1 \to 2 \to 3 \to 4 \to 1$ of all indices in the last equation.

E Abbreviations

bcc	body-centered cubic
BZ	Brillouin zone
DFT	Density Functional Theory
EMD	electron momentum density
FEG	free electron gas
FT	Fourier Transform
GTO	Gaussian Type Orbital
GTOFF	GTO's with Fitting Functions
GW	product of the Green's function G by the screened potential W
hcp	hexagonal close packed
IBZ	irreducible Brillouin zone
KK	Kramers–Kronig
KS	Kohn–Sham
LDA	Local Density Approximation (within DFT)
LFE	local field effect
LPDA	Local Plasma Density Approximation (to the stopping power)
PW	plane wave
RPA	Random Phase Approximation
SI	Système Internationale
UC	unit cell

References

[1] A.R. Lubinsky, D.E. Ellis, G.S. Painter, Phys. Rev. B 6 (1972) 3950.

[2] S.P. Singhal, Phys. Rev. B 12 (1975) 564.

[3] W.Y. Ching, J. Callaway, Phys. Rev. B 9 (1974) 5115.

[4] G. Cappellini, R. Del Sole, L. Reining, F. Bechstedt, Phys. Rev. B 47 (1993) 9892.

[5] A. Baldereschi, E. Tosatti, Phys. Rev. B 17 (1978) 4710.

[6] M.S. Hybertsen, S.G. Louie, Adv. Quantum Chem. 21 (1990) 155.

[7] L. Fritsche, Y.M. Gu, Phys. Rev. B 48 (1993) 4250.

[8] S. Massidda, A. Continenza, M. Posternak, A. Baldereschi, Phys. Rev. B 55 (1997) 13494.

[9] A. Schindlmayr, R.W. Godby, Phys. Rev. Lett. 80 (1998) 1702.

[10] J. Lindhard, A. Winther, K. Dan. Vidensk. Selsk. Mat. Fys. Medd. 34 (4) (1964).

[11] M. Kitagawa, Vacuum 39 (1989) 335.

[12] W. Brandt, Nucl. Instrum. Methods 194 (1982) 13.

[13] W. Brandt, M. Kitagawa, Phys. Rev. B 25 (1982) 5631.

[14] W. Brandt, M. Kitagawa, Phys. Rev. B 26 (1982) 3968(E).

[15] T. Kaneko, Phys. Status Solidi B 156 (1989) 49.

[16] T. Kaneko, Phys. Rev. A 40 (1989) 2188.

[17] T. Kaneko, At. Data Nucl. Data Tables 53 (1993) 271.

[18] P.M. Echenique, M.E. Uranga in Interaction of Charged Particles with Solids and Surfaces, edited by A. Gras-Martí, H.M. Urbassek, N.R. Arista, F. Flores (Plenum Press, NY, 1991).

[19] P.W.L. van Dijk, L.J. van IJzendoorn, M. de Koning, P. Bobbert, W. van Haeringen, M.J.A. de Voigt, Nucl. Instrum. Methods B 85 (1994) 551.

[20] J.A. Nobel, J.R. Sabin, S.B. Trickey, Nucl. Instrum. Methods B 99 (1995) 632.

[21] J. Calera-Rubio, A. Gras-Martí, N.R. Arista, Nucl. Instrum. Methods B 93 (1994) 137.

[22] K.M. Klein, C. Park, A.F. Tasch, Appl. Phys. Lett. 57 (1990) 2701.

[23] S.T. Nakagawa, Phys. Status Solidi B 178 (1993) 87.

[24] K. Lenkheit, Ch. Trikalinos, L.L. Balashova, N.M. Kabashnik, V.I. Shulga, Phys. Status Solidi B 161 (1990) 513.

[25] D. Cai, N. Grønbech-Jensen, C.M. Snell, K.M. Beardmore, Phys. Rev. B 54 (1996) 17147.

[26] W. Neng-ping, H. Yu-kun, Phys. Rev. A 52 (1995) 3953.

[27] P. Vargas, J.E. Valdés, N.R. Arista, Phys. Rev. A 53 (1996) 1638.

[28] P. Vargas, J.E. Valdés, N.R. Arista, J. Phys. B 29 (1996) 47.

[29] H. Tups, K. Syassen, J. Phys. F 14 (1984) 2753.

[30] V.L. Moruzzi, J.F. Janak, A.R. Williams, Calculated Electronic Properties of Metals, (Pergamon, New York, 1978).

[31] J.W. Mintmire, J.R. Sabin, S.B. Trickey, Phys. Rev. B 26 (1982) 1743.

[32] U. Birkenheuer, J.C. Boettger, N. Rösch, J. Chem. Phys. 100 (1994) 6826.

[33] J.C. Boettger, S.B. Trickey, Phys. Rev. B 53 (1996) 3007.

[34] J.C. Boettger, J.M. Wills, Phys. Rev. B 54 (1996) 8965.

[35] J.C. Boettger, Phys. Rev. B 55 (1997) 750.

[36] J.C. Boettger, Phys. Rev. B 55 (1997) 11202.

[37] B.I. Dunlap, J. Andzelm, J.W. Mintmire, Phys. Rev. A 42 (1990) 6354.

[38] J.E. Jaffe, A.C. Hess, J. Chem. Phys. 105 (1996) 10983.

[39] S.K. Goh, A. St-Amant, Chem. Phys. Lett. 264 (1997) 9.

[40] L. Serra, A. Rubio, Phys. Rev. Lett. 78 (1997) 1428.

[41] P. Duffy, D.P. Chong, M.E. Casida, D.R. Salahub, Phys. Rev. A 50 (1994) 4707.

[42] A.G. Eguiluz, Int. J. Quantum Chem. 60 (1996) 1457.

[43] P. Duffy, Can. J. Phys. 74 (1996) 763.

[44] S.L. Adler, Phys. Rev. 126 (1962) 413.

[45] O.V. Dolgov, E.G. Maksimov in The Dielectric Function of Condensed Systems, vol. 24 of Modern Problems in Condensed Matter Sciences, edited by L.V. Keldysh, D.A. Kirzhnitz, A.A. Maradudin (North-Holland, Amsterdam, 1989), Chap. 4.

[46] N. Wiser, Phys. Rev. 129 (1963) 62.

[47] V.I. Gavrilenko, F. Bechstedt, Phys. Rev. B 55 (1997) 4343.

[48] D.S. Falk, Phys. Rev. 118 (1960) 105.

[49] F. Aryasetiawan, O. Gunnarsson, Phys. Rev. B 49 (1994) 16214.

[50] X. Blase, A. Rubio, S.G. Louie, M.L. Cohen, Phys. Rev. B 52 (1995) R2225.

[51] R. Ahuja, S. Auluck, J.M. Wills, M. Alouani, B. Johansson, O. Eriksson, Phys. Rev. B 55 (1997) 4999.

[52] R. Ahuja, S. Auluck, J.M. Wills, M. Alouani, B. Johansson, O. Eriksson, Phys. Rev. B 56 (1997) 12652(E).

[53] E.H. Mortensen, J. Oddershede, J.R. Sabin, Nucl. Instrum. Methods B 69 (1992) 24.

[54] D. Ayma, J.P. Campillo, M. Rérat, M. Causà, J. Comput. Chem. 18 (1997) 1253.

[55] D. Ayma, M. Rérat, A. Lichanot, J. Phys.: Condens. Matter 10 (1998) 557.

[56] P.M. Echenique, F.J. García de Abajo, V.H. Ponce, M.E. Uranga, Nucl. Instrum. Methods B 96 (1995) 583.

[57] A. Cohen Simonsen, F. Yubero, S. Tougaard, Phys. Rev. B 56 (1997) 1612.

[58] J. Osma, P.M. Echenique, N. Mårtensson, Phys. Rev. B 56 (1997) 3644.

[59] H. Ishida, Phys. Rev. B 57 (1998) 4140.

[60] J. Lindhard, K. Dan. Vidensk. Selsk. Mat. Fys. Medd. 28 (8) (1954).

[61] J. Berger, S.G. Eckstein, Phys. Rev. B 26 (1982) 4305.

[62] R.A. Evarestov, V.P. Smirnov, Site Symmetry in Crystals, Springer Series in Solid-State Sciences, ed. by M. Cardona vol. 108 (Springer, Berlin, 1993), Eq. (3.8.9).

[63] P.J.H. Denteneer, W. van Haeringen, J. Phys. C 18 (1985) 4127; eq. (3.6.5) in [64].

[64] J. Callaway, Quantum Theory of the Solid State, (Academic Press, New York, 1974).

[65] W.M. Saslow, G.F. Reiter, Phys. Rev. B 7 (1973) 2995.

[66] M.S. Hybertsen, S.G. Louie, Phys. Rev. B 35 (1987) 5585.

[67] N. Hamada, M. Hwang, A.J. Freeman, Phys. Rev. B 41 (1990) 3620.

[68] R. Resta, A. Baldereschi, Phys. Rev. B 23 (1981) 6615.

[69] A.F. Burenkov, F.F. Komarov, M.A. Kumakhov, Phys. Status Solidi B 99 (1980) 417.

[70] L.R. Logan, C.S. Murthy, G.R. Srinivasan, Phys. Rev. A 46 (1992) 5754.

[71] F. Bonsignori, A. Desalvo, J. Phys. Chem. Solids 31 (1970) 2191.

[72] A. Desalvo, R. Rosa, J. Phys. C 10 (1977) 1595.

[73] T.M.H. Tielens, G.E.W. Bauer, T.H. Stoof, Phys. Rev. B 49 (1994) 5741.

[74] O.H. Crawford, C.W. Nestor, Jr., Phys. Rev. A 28 (1983) 1260.

[75] M. Zaider, D.E. Orr, J.L. Fry, Int. J. Supercomp. Appl. 4 (1990) 25.

[76] W. von der Linden, P. Horsch, Phys. Rev. B 37 (1988) 8351.

[77] D.L. Johnson, Phys. Rev. B 9 (1974) 4475.

[78] A.J. Forsyth, T.W. Josefsson, A.E. Smith, Phys. Rev. B 54 (1996) 14355.

[79] J. d'Albuquerque e Castro, R. Bechara Muniz, L.E. Oliveira, Phys. Status Solidi B 158 (1990) 743.

[80] T. Živković, Z.B. Maksić, J. Chem. Phys. 49 (1968) 3083.

[81] R. Lindh, U. Ryu, B. Liu, J. Chem. Phys. 95 (1991) 5889.

[82] W. Klopper, R. Röhse, Theor. Chim. Acta 83 (1992) 441.

[83] T. Helgaker, P.R. Taylor, Chapt. 12 in Modern Electronic Structure Theory, edited by D.R. Yarkony (World Scientific, Singapore, 1995).

[84] Z.H. Levine, D.C. Allan, Phys. Rev. B 43 (1991) 4187.

[85] V. Fiorentini, A. Baldereschi, Phys. Rev. B 51 (1995) 17196.

[86] Z.H. Levine, Int. J. Quantum Chem. Symp. 28 (1994) 411.

[87] B. Adolph, V.I. Gavrilenko, K. Tenelsen, F. Bechstedt, R. Del Sole, Phys. Rev. B 53 (1996) 9797.

[88] R. Resta, Phys. Rev. Lett. 77 (1996) 2265.

[89] W.G. Aulbur, L. Jönsson, J.W. Wilkins, Phys. Rev. B 54 (1996) 8540.

[90] R.M. Martin, G. Ortiz, Phys. Rev. B 56 (1997) 1124.

[91] G. Ortiz, I. Souza, R.M. Martin, Phys. Rev. Lett. 80 (1998) 353.

[92] F. Bechstedt, K. Tenelsen, B. Adolph, R. Del Sole, Phys. Rev. Lett. 78 (1997) 1528.

[93] A.A. Quong, A.G. Eguiluz, Phys. Rev. Lett. 70 (1993) 3955.

[94] F. Catara, G. Piccitto, M. Sambataro, N. Van Giai, Phys. Rev. B 54 (1996) 17536.

[95] J. Schirmer, F. Mertins, J. Phys. B 29 (1996) 3559.

[96] R.J. Mathar, Phys. Rev. A 53 (1996) 2873.

[97] R. Cenni, F. Conte, A. Cornacchia, P. Saracco, Riv. Nuovo Cimento 15, No. 12 (1992).

[98] R. Colle, A. Fortunelli, S. Simonucci, Nuovo Cimento 9D (1987) 969.

[99] P. Kaijser, V.H. Smith Jr, Adv. Quantum Chem. 10 (1977) 37.

[100] P. Čársky, V. Hronda, M. Polášek, Theor. Chim. Acta 93 (1996) 49.

[101] J.P.A. Charlesworth, W. Yeung, Comput. Phys. Commun. 88 (1995) 186.

[102] J.P.A. Charlesworth, W. Yeung, Phys. Rev. B 53 (1996) 2606.

[103] J. Rath, A.J. Freeman, Phys. Rev. B 11 (1975) 2109.

[104] P.-A. Lindgård, Solid State Commun. 16 (1975) 481.

[105] R.L. Jacobs, D. Lipton, in Computational Methods in Band Theory, edited by P.B. Marcus, J.F. Janak, A.R. Williams (Plenum, New York, 1971), p. 340.

[106] J.B. Diamond, in Computational Methods in Band Theory, edited by P.B. Marcus, J.F. Janak, A.R. Williams (Plenum, New York, 1971), p. 347.

[107] P.E. Blöchl, O. Jepsen, O.K. Andersen, Phys. Rev. B 49 (1994) 16223.

[108] W. Yeung, J. Phys.: Condens. Matter 4 (1992) L467.

[109] O. Jepsen, O.K. Andersen, Phys. Rev. B 29 (1984) 5965.

[110] B. Farid, D. Lenstra, W. van Haeringen, Solid State Commun. 67 (1988) 7.

[111] A.D. Zdetsis, Phys. Rev. B 34 (1986) 7666.

[112] R. Berliner, S.A. Werner, Phys. Rev. B 34 (1986) 3586.

[113] J.C. Boettger, S.B. Trickey, J.A. Nobel, Phys. Rev. B 45 (1992) 7503.

[114] J.A. Nobel, S.B. Trickey, P. Blaha, K. Schwarz, Phys. Rev. B 45 (1992) 5012.

[115] R. Ahuja, S. Auluck, J.M. Wills, O. Eriksson, P. Söderlind, B. Johansson, Phys. Rev. B 50 (1994) 18003.

[116] J.-H. Cho, S.-H. Ihm, M.-H. Kang, Phys. Rev. B 47 (1993) 14020.

[117] W. Schwarz, O. Blaschko, I. Gorgas, Phys. Rev. B 44 (1991) 6785.

[118] P. Staikov, A. Kara, T.S. Rahman, J. Phys.: Condens. Matter 9 (1997) 2135.

[119] N. Tugluoglu, R.H. Mutlu, Phys. Rev. B 54 (1996) 10253

[120] N. Tugluoglu, R.H. Mutlu, Phys. Rev. B 56 (1997) 12651(E).

[121] K. Sturm, Adv. Phys. 31 (1982) 1.

[122] W. Schülke, H. Nagasawa, S. Mourikis, P. Lanzki, Phys. Rev. B 33 (1986) 6744.

[123] Y.-G. Jin, K.J. Chang, Phys. Rev. B 57 (1998) 14684.

[124] H. Eckstein, W. Schattke, Physica A 216 (1995) 151.

[125] K. Kokko, P.T. Salo, R. Laihia, K. Mansikka, Phys. Rev. B 52 (1995) 1536.

[126] K. Kokko, P.T. Salo, R. Laihia, K. Mansikka, Surf. Sci. 348 (1996) 168.

[127] T. Kotani, H. Akai, Phys. Rev. B 52 (1995) 17153.

[128] Y. Kubo, J. Phys. Soc. Japan 65 (1996) 16.

[129] H. Bross, M. Ehrnsperger, Z. Phys. B 97 (1995) 17.

[130] J.C. Boettger, S.B. Trickey, Phys. Rev. B 45 (1992) 1363.

[131] K. Karlsson, F. Aryasetiawan, Phys. Rev. B 52 (1995) 4823.

[132] E. Knittle, R.M. Wentzcovitch, R. Jeanloz, M.L. Cohen, Nature 337 (1989) 349

[133] L. Lam, P.M. Platzman, Phys. Rev. B 9 (1974) 5122.

[134] L. Lam, P.M. Platzman, Phys. Rev. B 9 (1974) 5128.

[135] G.E.W. Bauer, Phys. Rev. B 27 (1983) 5912.

[136] A. Görling, M. Levy, J.P. Perdew, Phys. Rev. B 47 (1993) 1167.

[137] M. Taut, J. Phys. C 18 (1985) 2677.

[138] M. Tuat, J. Phys. C 18 (1985) 2691.

[139] K. Sturm, Phys. Rev. B 52 (1995) 8028.

[140] G. Lévêque, Phys. Rev. B 34 (1986) 5070.

[141] G.D. Mahan, Many-Particle Physics, 2nd ed. (Plenum, New York, London, 1990), chapt. 5.7.

[142] E. Hadjimichael, W. Currie, S. Fallieros, Am. J. Phys. 65 (1997) 335.

[143] P. Alippi, P. La Rocca, G.B. Bachelet, Phys. Rev. B 55 (1997) 13835.

[144] S. Scandolo, F. Bassani, Phys. Rev. B 51 (1995) 6925.

[145] M. Alouani, J.M. Wills, Phys. Rev. B 54 (1996) 2480.

[146] G.J. Iafrate, J.F. Ziegler, J. Appl. Phys. 50 (1979) 5579.

[147] N. Durante, U.T. Lamanna, G.P. Arrighini, C. Guidotti, Theor. Chim. Acta 90 (1995) 115.

[148] K.-H. Lee, K.J. Chang, Phys. Rev. B 49 (1994) 2362.

[149] J. Oddershede, J.R. Sabin, Nucl. Instrum. Methods B 48 (1990) 34.

[150] J.M. Pitarke, Phys. Rev. B 52 (1995) 13883.

[151] N.M. Kabachnik, J. Phys. B 26 (1993) 3803.

[152] P.L. Grande, G. Schiwietz, Phys. Lett. A 163 (1992) 439.

[153] P. Sigmund, Phys. Rev. A 26 (1982) 2497.

[154] P.M. Echenique, Nucl. Instrum. Methods B 27 (1987) 256.

[155] I. Nagy, J. László, J. Giber, Nucl. Instrum. Methods B 27 (1987) 276.

[156] E. Zaremba, A. Arnau, P.M. Echenique, Nucl. Instrum. Methods B 96 (1995) 619.

[157] M. Vaccari, A. Ventura, Nuovo Cimento 18D (1996) 69.

[158] Y.-N. Wang, T.-C. Ma, Phys. Rev. A 55 (1997) 2087.

[159] J.E. Valdés, J.C. Eckardt, G.H. Lantschner, N.R. Arista, Phys. Rev. A 49 (1994) 1083.

[160] H. Daniel, F.J. Hartmann, W. Neumann, W. Schott, Phys. Lett. A 191 (1994) 155.

[161] R. Golser, D. Semrad, Phys. Rev. Lett. 66 (1991) 1831.

[162] E. Morenzoni, Th. Prokscha, A. Hofer, B. Matthias, M. Meyberg, Th. Wutzke, H. Glückler, M. Birke, J. Litterst, Ch. Neidermayer, G. Schatz, J. Appl. Phys. 81 (1997) 3340.

[163] R.J. Mathar, M. Posselt, Phys. Rev. B 51 (1995) 15798.

[164] I.S. Tilinin, Phys. Rev. A 51 (1995) 3058.

[165] P. Sigmund, Phys. Rev. A 54 (1996) 3113.

[166] G. Schiwietz, P.L. Grande, Nucl. Instrum. Methods B 90 (1994) 10.

[167] A. Belkacem, P. Sigmund, Nucl. Instrum. Methods B 48 (1990) 29.

[168] A. Arnau, P.M. Echenique, R.H. Ritchie, Nucl. Instrum. Methods B 33 (1988) 138.

[169] M. Inokuti, Rev. Mod. Phys. 43 (1971) 297.

[170] M. Inokuti, Y. Hikawa, J.E. Turner, Rev. Mod. Phys. 50 (1978) 23.

[171] K. Dettmann, Z. Physik A 272 (1975) 227.

[172] K. Eder, D. Semrad, P. Bauer, R. Golser, P. Maier-Komor, F. Aumayr, M. Peñalba, A. Arnau, J.M. Ugalde, P.M. Echenique, Phys. Rev. Lett. 79 (1997) 4112.

[173] J.-Z. Wu, S.B. Trickey, J.R. Sabin, Nucl. Instrum. Methods B 79 (1993) 206.

[174] J.Z. Wu, S.B. Trickey, J.R. Sabin, J.C. Boettger, Phys. Rev. B 51 (1995) 14576.

[175] J.Z. Wu, S.B. Trickey, J.R. Sabin, J.C. Boettger, Phys. Rev. B 58 (1998) 4182(E).

[176] S.B. Trickey, J.Z. Wu, J.R. Sabin, Nucl. Instrum. Methods B 93 (1994) 186.

[177] R.J. Mathar, Nucl. Instrum. Methods B 132 (1997) 18.

[178] I. Campillo, J.M. Pitarke, A.G. Eguiluz, A. García, Nucl. Instrum. Methods B 135 (1998) 103.

[179] G. Gumbs, N.J.M. Horing, Phys. Rev. B 43 (1991) 2119.

[180] M. Šunjić, A.A. Lucas, Phys. Rev. B 3 (1971) 719.

[181] Z. Pensar, M. Šunjić, Phys. Scr. 30 (1984) 431.

[182] P. Sigmund, Nucl. Instrum. Methods B 95 (1995) 477.

[183] L.E. Porter, Phys. Rev. A 50 (1994) 2397.

[184] L.E. Porter, Int. J. Quantum Chem. 65 (1997) 997.

[185] C. Bradley, A.P. Cracknell, Mathematical Theory of the Group Symmetry in Solids, (Clarendon, Oxford, 1972).

[186] D.A. Kirzhnitz in The Dielectric Function of Condensed Systems, vol. 24 of Modern Problems in Condensed Matter Sciences, edited by L.V. Keldysh, D.A. Kirzhnitz, A.A. Maradudin (North-Holland, Amsterdam, 1989).

[187] C.W. Peterson, B.W. Knight, J. Opt. Soc. Am. 63 (1973) 1238.

[188] B.I. Dunlap, J.C. Boettger, J. Phys. B 29 (1996) 4907.

[189] R. Haensel, C. Kunz, B. Sonntag, Phys. Rev. Lett. 20 (1968) 262.

[190] G.K. Wertheim, D.M. Riffe, P.H. Citrin, Phys. Rev. B 45 (1992) 8703.

[191] J.P. Worth, C.L. Merry, S.B. Trickey, J. Phys. Chem. Solids 41 (1980) 623.

[192] D. Mearns, W. Kohn, Phys. Rev. B 39 (1989) 10669.

[193] N.I. Papanicolaou, N.C. Bacalis, D.A. Papaconstantopoulos, Handbook of Calculated Electron Momentum Distributions, Compton Profiles, and X-ray Form Factors of Elemental Solids, (CRC Press, Boca Raton, 1991).

[194] Y. Sakurai, Y. Tanaka, A. Bansil, S. Kaprzyk, A. T. Stewart, Y. Nagashima, T. Hyodo, S. Nanao, H. Kawata, N. Shiotani, Phys. Rev. Lett. 74 (1995) 2252.

[195] Ch. Eppacher, R. Díez Muiño, D. Semrad, A. Arnau, Nucl. Instrum. Methods B 96 (1995) 639.

[196] J.F. Janni, At. Data Nucl. Data Tables 27 (1982) 147.

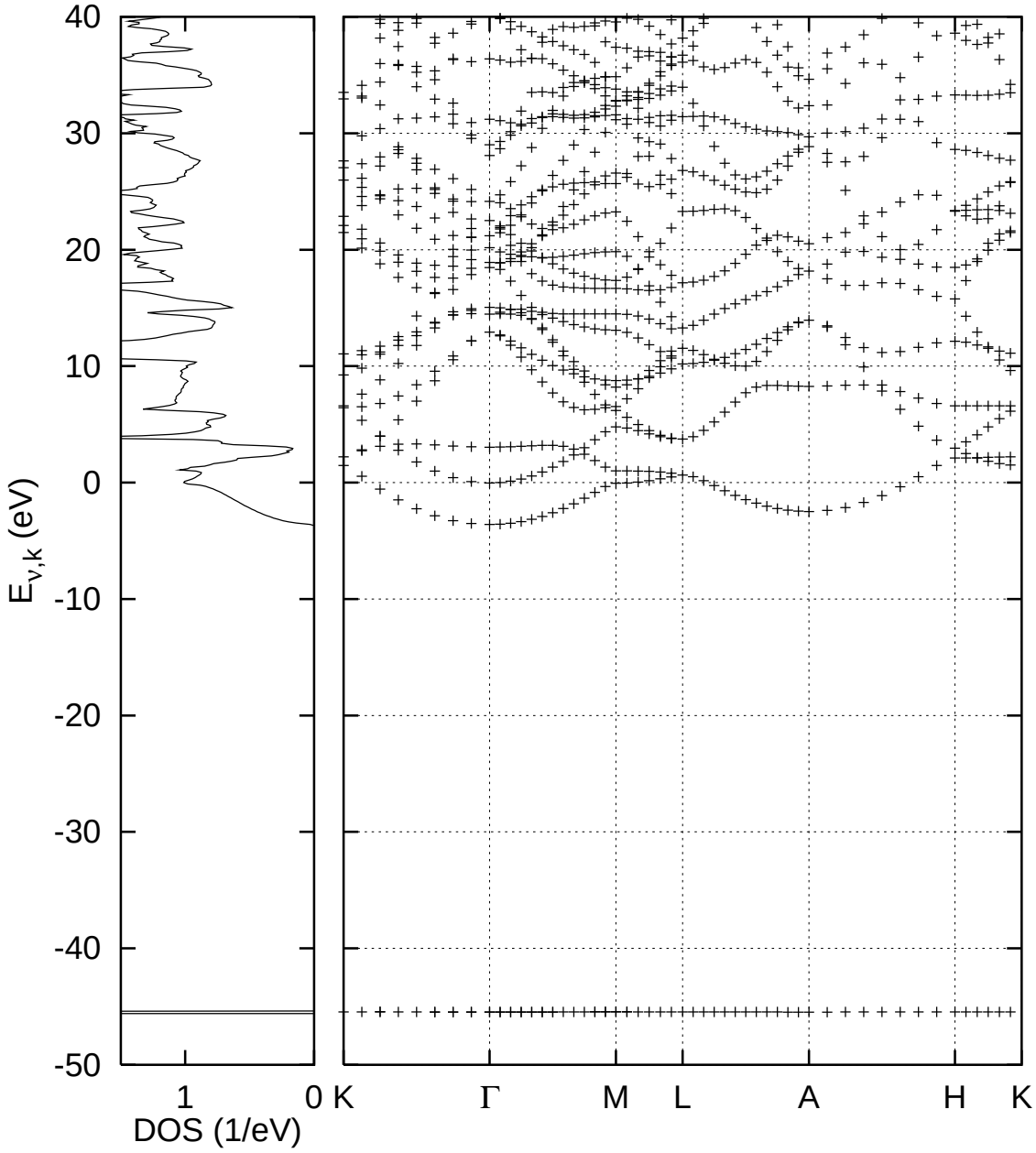

Fig. 1. Band-structure $E_{\nu,\mathbf{k}}$ of hcp lithium at lattice parameters $a = 5.65a_0$ and $c = 9.26a_0$ [173] from GTOFF. E_F is set to 0 eV. This run used $24 \times 24 \times 12$ $\mathbf{k}$-points in the BZ, that is 427 in the IBZ. The experimental value of the K-edge is about 10 eV lower than calculated here [189,190].

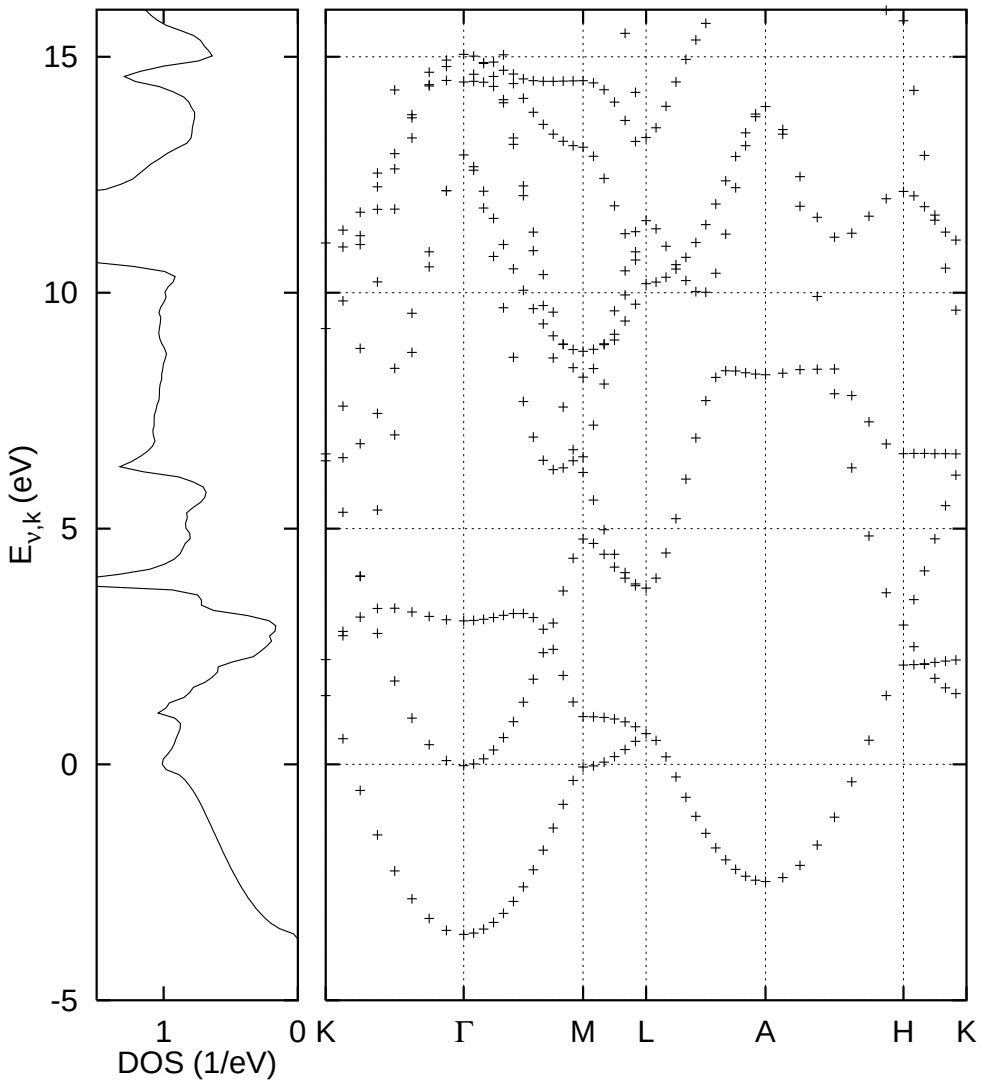

Fig. 2. Magnified view of Fig. 1.

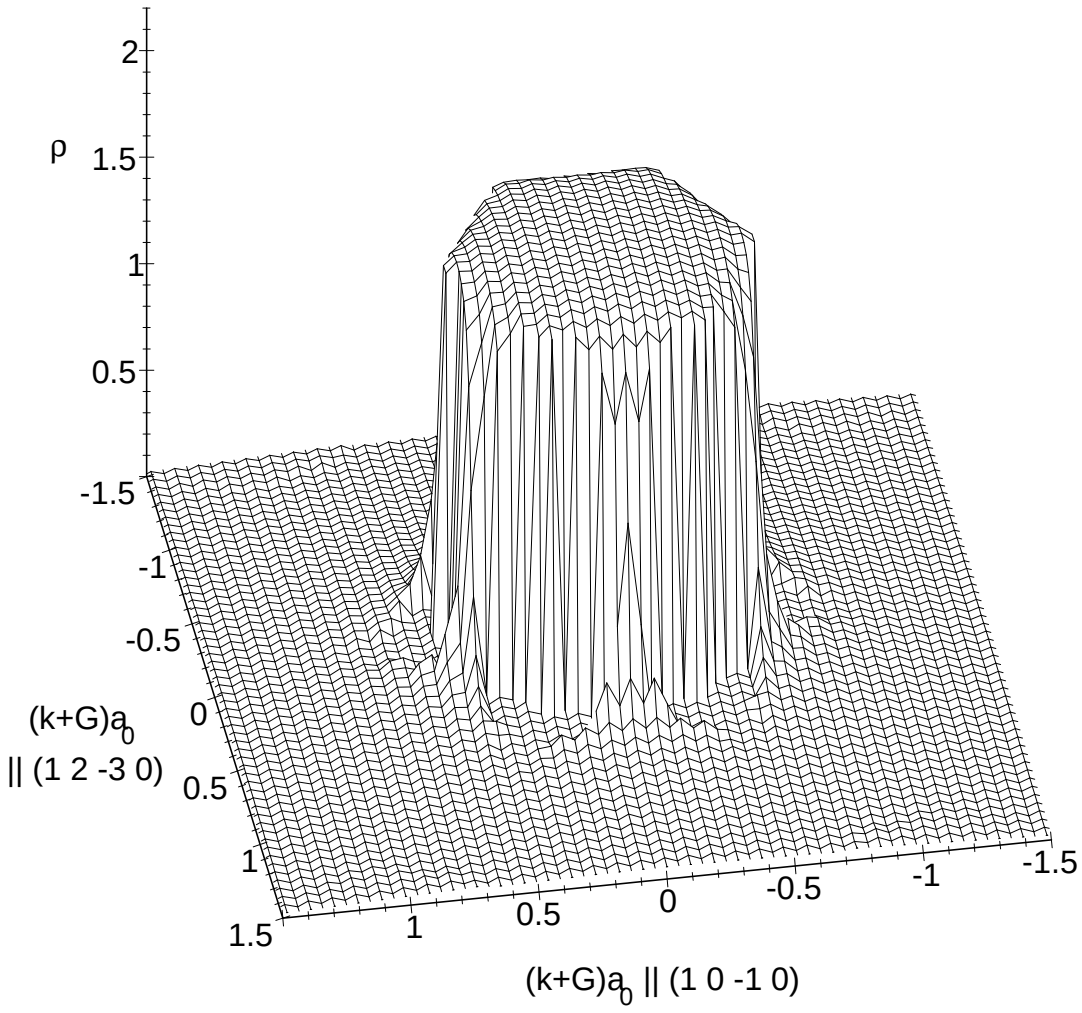

Fig. 3. The EMD [191] of hexagonal lithium as a function of $\mathbf{k} + \mathbf{G}$, which is varied in the plane spanned by $(10\bar{1}0)$ and $(12\bar{3}0)$. Both momentum components are measured in units of $1/a_0$ (reciprocal Bohr radii, atomic units). The relationship between the EMD and the Fermi surface has been discussed by Mearns and Kohn [192].

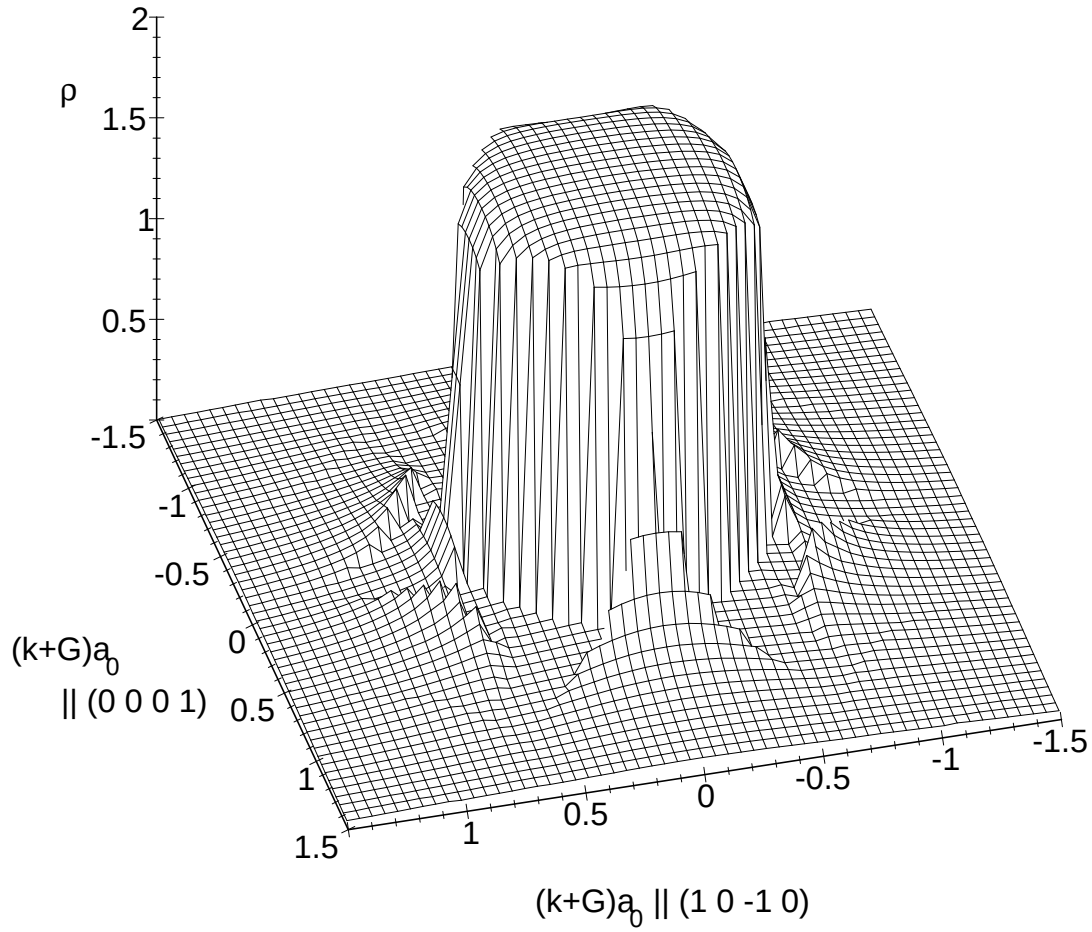

Fig. 4. The EMD of hexagonal lithium as a function of $\mathbf{k} + \mathbf{G}$, varied in the plane spanned by $(10\bar{1}0)$ and (0001). Where the BZ surfaces meet the Fermi surface, pieces are sheared off the Fermi ice block and drift as nearby floes. See [193,194] for the bcc phase.

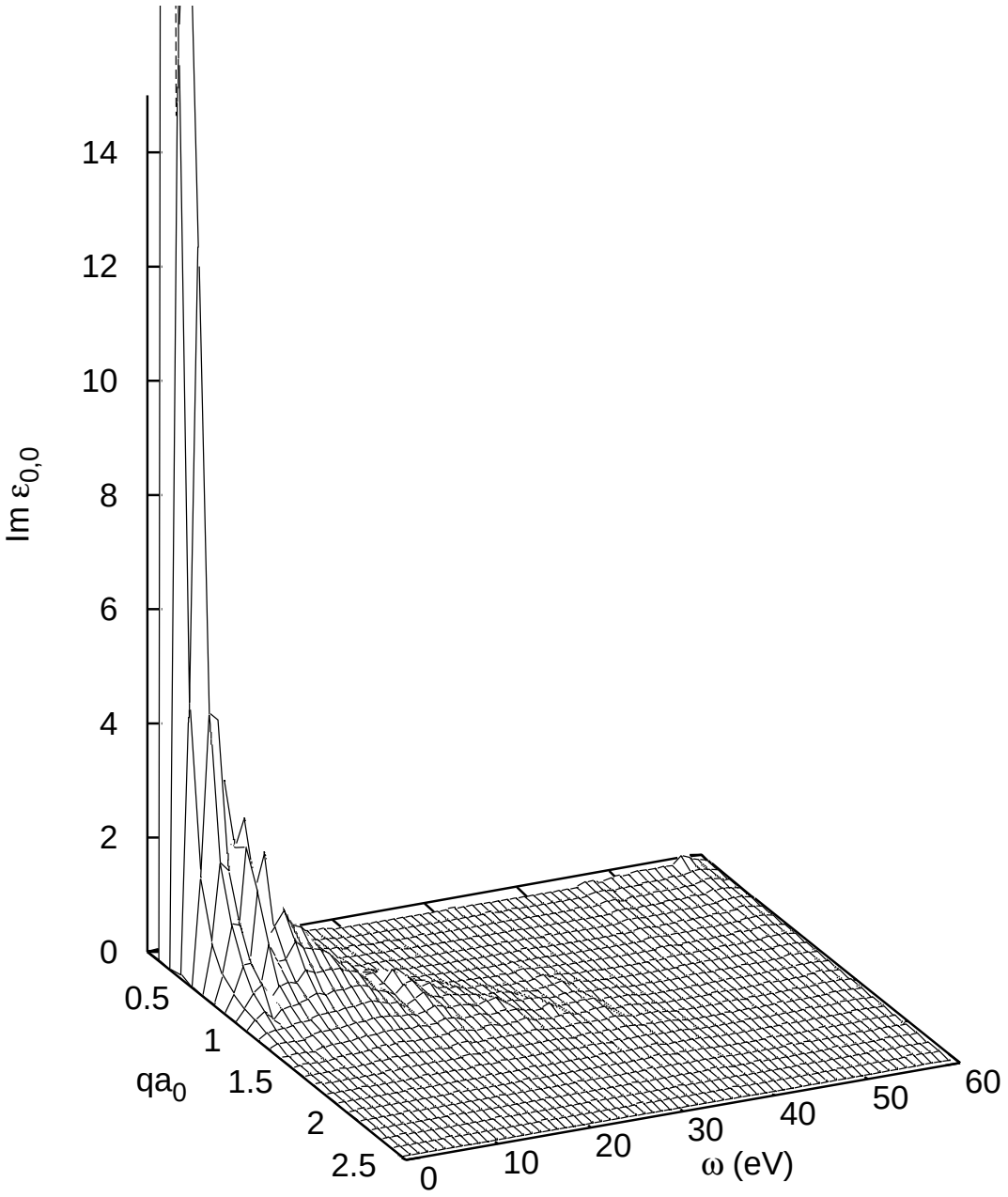

Fig. 5. Calculated $\mathrm{Im}\,\epsilon_{\mathbf{G},\mathbf{G}'}$ of hcp Li for $\mathbf{G} = \mathbf{G}' = \mathbf{0}$. $\mathbf{q} \parallel (10\bar{1}0)$. Figs. 5–7 have been calculated starting from a DFT input with $12 \times 12 \times 6$ $\mathbf{k}$-points in the BZ (76 points in the IBZ).

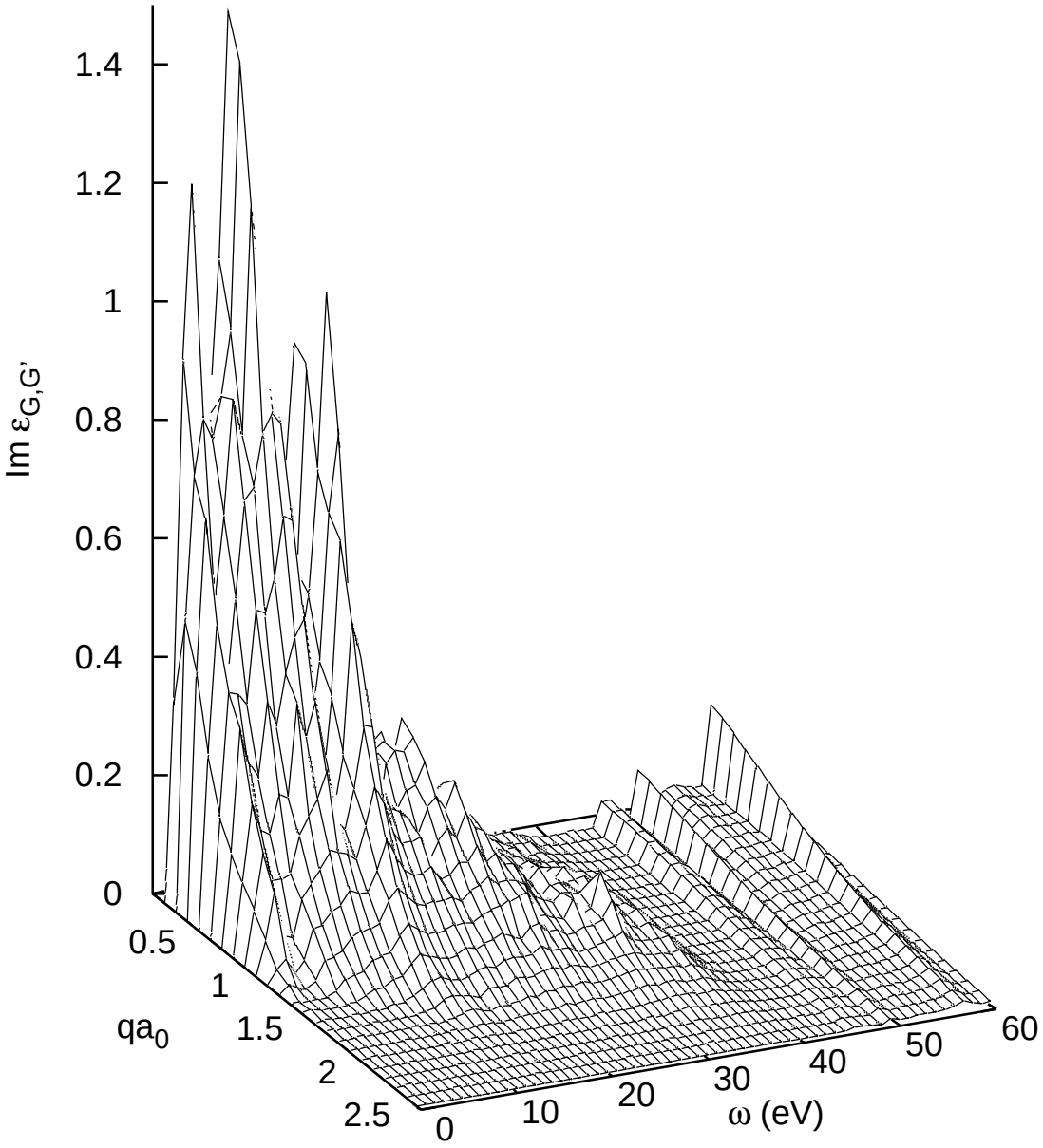

Fig. 6. Im $\epsilon_{\mathbf{G},\mathbf{G}'}$ of hcp lithium for $\mathbf{G} = \mathbf{G}' = (0001)$. $\mathbf{q} \parallel (10\bar{1}0)$.

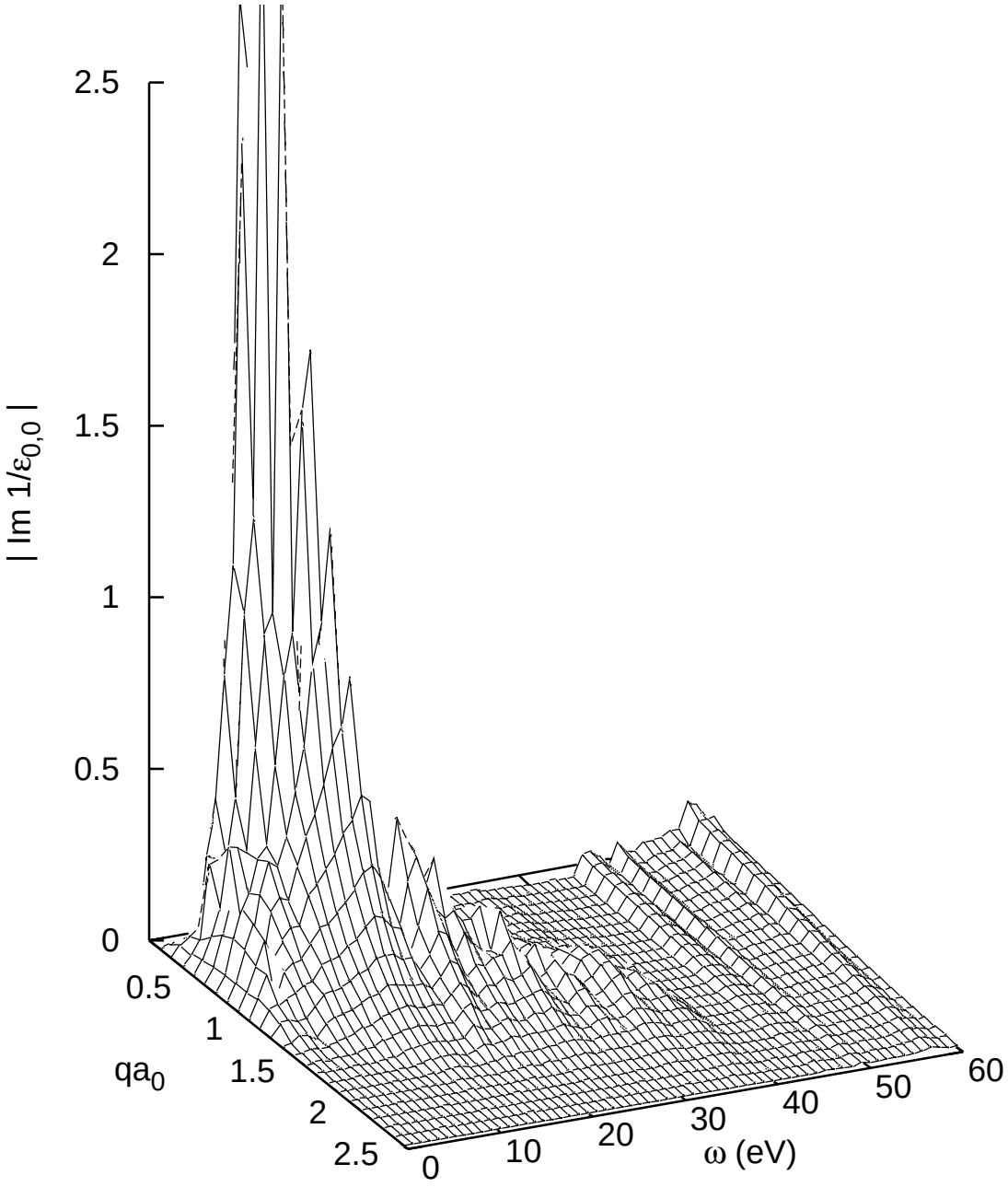

Fig. 7. Absolute value of $\mathrm{Im}[1/\epsilon_{\mathbf{0},\mathbf{0}}(\mathbf{q},\omega)]$ for hcp lithium. $\mathbf{q} \parallel (10\bar{1}0)$.

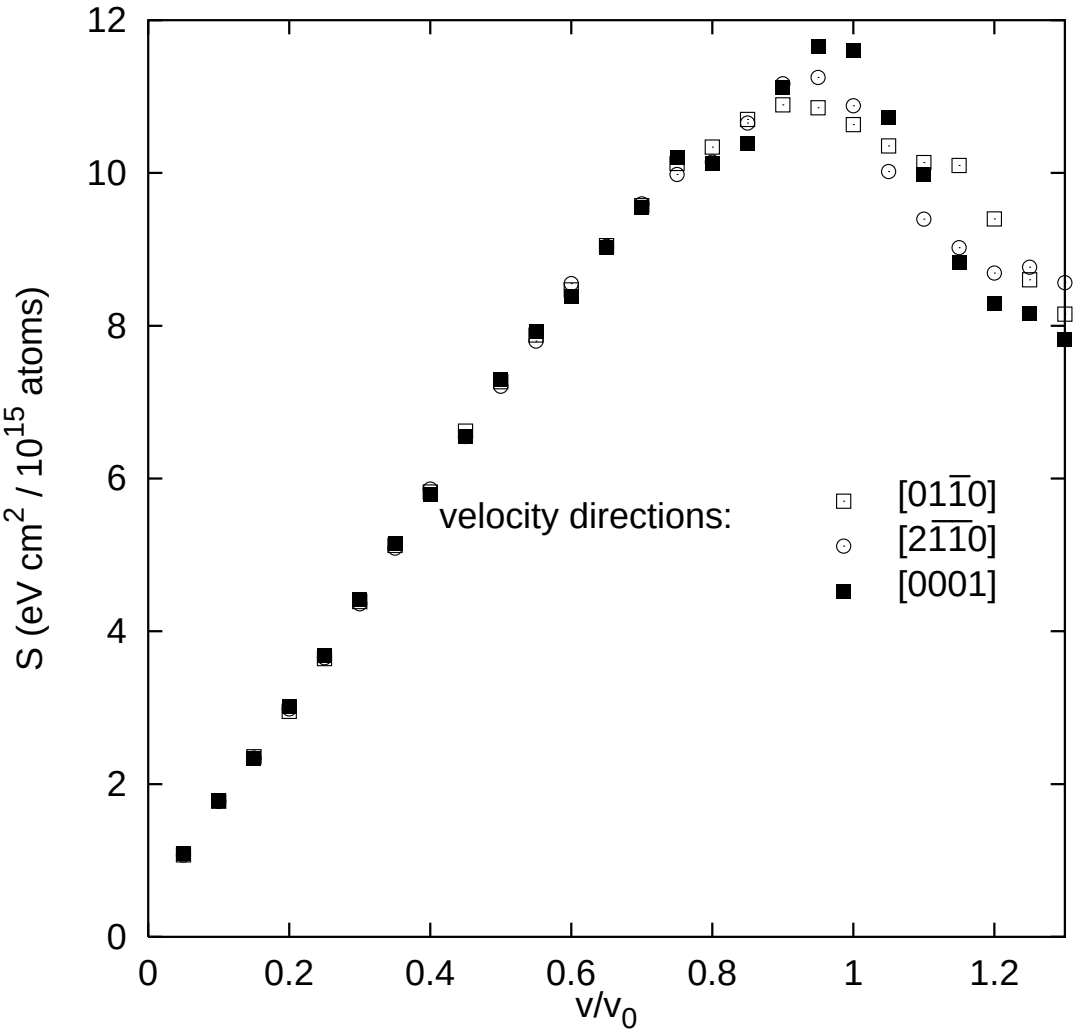

Fig. 8. Calculated lithium electronic stopping cross section. v_0 is the Bohr velocity. The energy loss function was integrated on a $27 \times 27 \times 33$ mesh in **q**-space (parallelepiped $5.6 \times 5.6 \times 5.4 a_0^{-3}$) and on a mesh with 64 points on the ω-axis ($0 \ldots 87$ eV). The lowest 24 bands were included in the sum over band-pairs in Eq. (7).

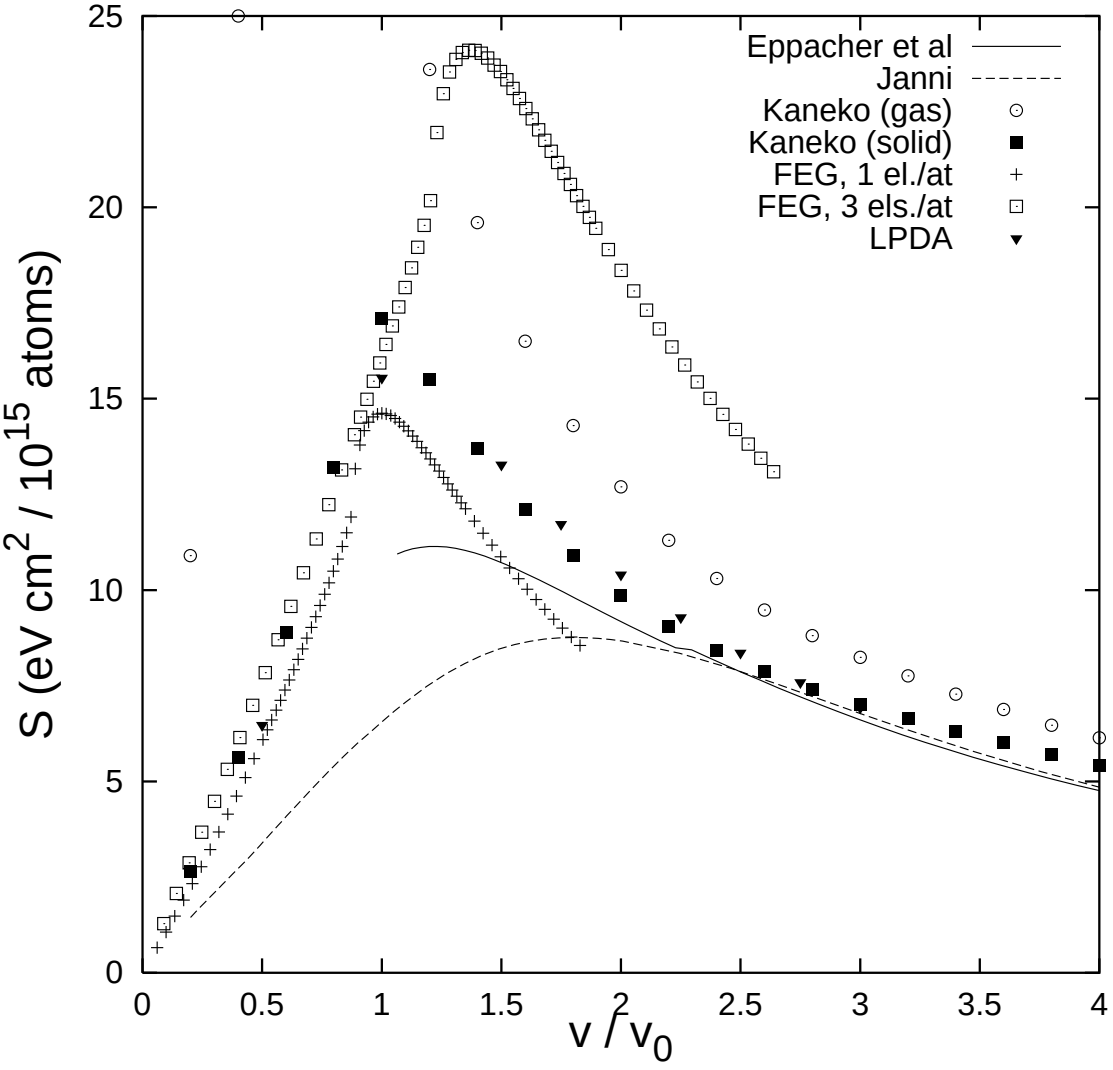

Fig. 9. Experimental proton stopping cross section of (probably bcc) Li by Eppacher *et al.* [195] and Janni [196], compared with calculated values for gaseous and solid Li from the Kaneko theory [15–17], and RPA free electron gas (FEG) values [10] with a homogeneous density equivalent to 1 or 3 electron(s) per Li atom (Fermi velocity $0.614v_0$ or $0.885v_0$) as shown. Values within the LPDA represent integrals of $\rho(\mathbf{r})$ of GTOFF Fitting Functions weighted with the Lindhard stopping number.

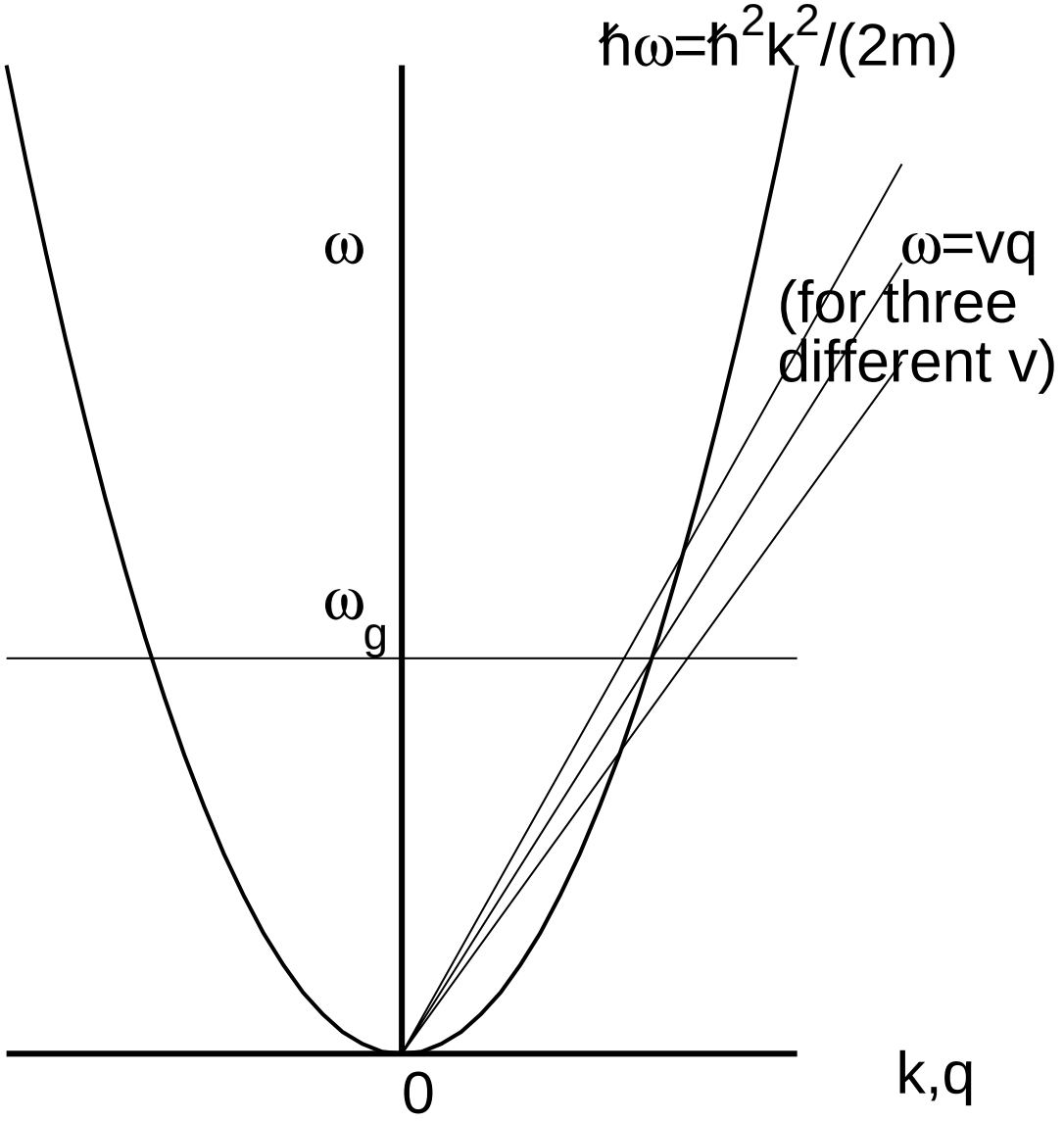

Fig. 10. The energy loss function has to be integrated over the triangular region Eq. (19), which simplifies for a homogeneous target to an integration over $0 \leq \omega \leq qv$. The figure shows the upper left boundary of this region for three different v (in relationship to a gap ω_g below, equal to, and above $v_0\sqrt{\hbar\omega_g/E_0}/2$ with increasing slope) in form of three straight lines through the origin. E_0 is 1 rydberg.

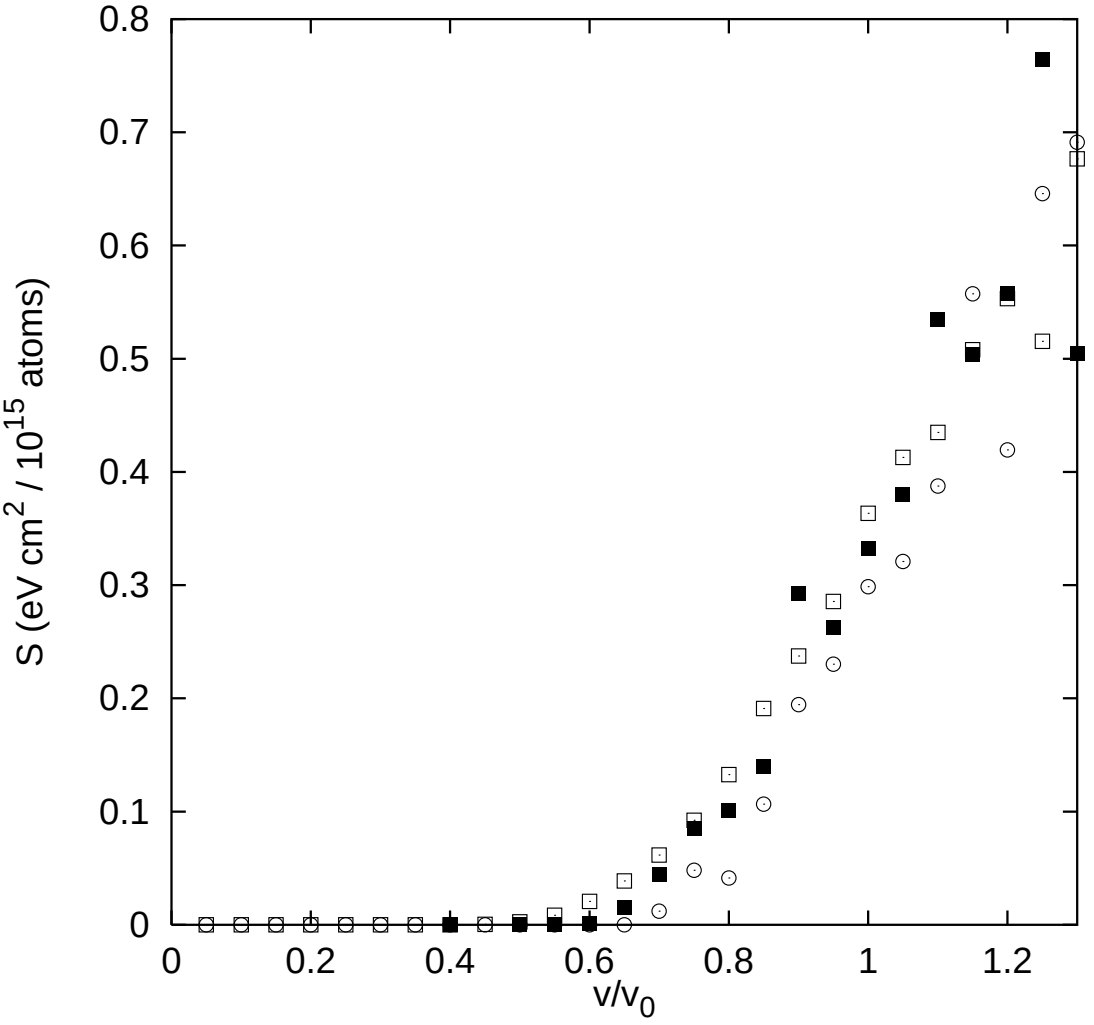

Fig. 11. If Π is calculated without contributions from the valence bands, i.e. with K-shell excitations alone, but with other parameters kept as in Fig. 8, the stopping cross section of hcp Li exhibits a non-linear behavior which reflects the effective band gap of $\hbar\omega_g \approx 45$ eV for this case; recall Fig. 1.